Swiss J Geosci (2014) 107:197–222
DOI 10.1007/s00015-014-0174-8

Continuity in geochemistry and time of the Tertiary Bergell intrusion (Central Alps)

Omar Gianola · Max W. Schmidt · Albrecht von Quadt · Irena Peytcheva · Pietro Luraschi · Eric Reusser

Received: 19 September 2013 / Accepted: 23 October 2014 / Published online: 3 December 2014

Abstract The calc-alkaline Bergell intrusion is classically mapped as a main tonalite and main granodiorite unit, whose ages have been determined at 32 and 30 Ma, respectively. These units are separated by a mostly thin band interpreted as magmatic "transition zone". High precision U–Pb dating of zircons and whole rock geochemistry of transition zone rocks are combined with a compilation of available geochemical analyses and ages to characterize the emplacement and magmatic evolution of the Bergell intrusion. Detailed field work shows that the transition zone is heterogeneous, characterized by multiple intrusions of tonalites to granodiorites to quartz-monzonites containing mafic enclaves and leucocratic dykes. Commonly, magmatic flow structures such as compositional banding, schlieren and accumulation of K-feldspar megacrystals are observed. The compositions of the transition zone intrusives as well as of the geochemically fairly heterogeneous tonalite and granodiorite units span a continuous range from 49–76 wt% SiO_2 for mafic enclaves to leucocratic dykes. Major and trace element trends are consistent with a predominant fractional crystallization. High precision U–Pb dating of single zircon grains separated from tonalites and granodiorites of the transition zone yields crystallization ages of 31.22 ± 0.04 and 31.13 ± 0.10 Ma, respectively. Hence, the transition zone represents an own phase of intrusion during which a range of magma types were coeval. The available ages and compositional data suggest magmatic activity over the entire range from 28 to 33 Ma across the Bergell intrusion, which should not be described by two main "tonalite" and "granodiorite" stages but by a model with several magmatic main phases during which most magma types developed multiply. Geobarometry of tonalite boulders in the Como molasse (yielding a zircon crystallization age of 32.06 ± 0.13 Ma) indicate average erosion rates for the Bergell intrusion of 1.9 mm/a between 32–25 Ma and of 0.5 mm/a since then.

Keywords Bergell transition zone · Como molasse · Erosion rate · U–Pb dating · Zircon · Zoned pluton

1 Introduction

Tertiary calc-alkaline mantle derived magmatism is frequent along the Periadriatic Fault System of the Alpine chain and ranges (east to west) from the Karawanken to the Rieserferner, Adamello and Bergell plutons to the Biella, Miagliano and Traversella intrusions (e.g. Cornelius 1915; Rosenberg 2004; Berger et al. 2012). The Bergell intrusion is the second largest of these magmatic bodies and, together with the Adamello batholith, represents the most studied of these plutons in terms of field relationships (e.g. Montrasio and Trommsdorff 1983; Trommsdorff and Nievergelt 1983), geochemistry (Reusser 1987; Diethelm 1989; von Blanckenburg et al. 1992), intrusion age (Gulson and Krogh 1973; von Blanckenburg 1989, 1992; Oberli et al. 2004), deformation history (Passerini et al. 1991; Berger and Stünitz 1996; Davidson et al. 1996) as well as

Electronic supplementary material The online version of this article (doi:10.1007/s00015-014-0174-8) contains supplementary material, which is available to authorized users.

O. Gianola (✉) · M. W. Schmidt · A. von Quadt · I. Peytcheva · P. Luraschi · E. Reusser
Department of Earth Sciences, Institute of Geochemistry and Petrology, ETH Zurich, Clausiusstrasse 25, 8092 Zurich, Switzerland
e-mail: omar.gianola@erdw.ethz.ch

emplacement temperatures and pressures (Reusser 1987; von Blanckenburg 1992; Davidson et al. 1996).

The Bergell intrusion is divided and mapped as three main parts or units: the tonalite, granodiorite and the "transition zone" (e.g. Moticska 1970; Berger 1996). More mafic compositions occur at the NW rim (mainly diorites and monzodiorites, Diethelm 1990) as well as at the NE rim of the Bergell intrusion (mostly hbl-gabbros and hornblendites, Diethelm 1989) and are frequent as mafic enclaves in all units. Furthermore, basaltic to shoshonitic dykes occur throughout the main body (Diethelm 1989). Mostly, the tonalite and granodiorite units are described as single large intrusives (e.g. Montrasio and Trommsdorff 1983; Trommsdorff and Nievergelt 1983; Reusser 1987) while the heterogeneity of the transition zone unit has been widely recognized (Moticska 1970; Wenk 1973; Reusser 1987; Davidson et al. 1996; Schmid et al. 1996). This heterogeneity has been interpreted to represent a zone of mixing and mingling of the two dominant units of the Bergell pluton, i.e. the main tonalite and the main granodiorite (Moticska 1970). Dating of the two main units in the eastern part of the intrusion resulted in ages of 31.9 ± 0.1 for the tonalite unit and 30.1 ± 0.2 for the granodiorite unit (von Blanckenburg 1992). The transition zone itself has not yet been systematically investigated both in terms of geochemistry and age.

Another magmatic body in close spatial but not geochemical relation to the calc-alkaline Bergell intrusion is the 24.0 ± 1.2 Ma Novate granite (Liati et al. 2000) which is strongly peraluminous and, from its trace elements and isotope geochemistry, an S-type granite derived from eutectic melting of the various surrounding gneissic units (von Blanckenburg et al. 1992). The Novate granite is in fact not a single large intrusive body but is composed by a multitude of dykes and stocks (of up to several 100 m in size) cutting across gneisses and also the calc-alkaline Bergell intrusion.

In this study, we investigated the transition zone by field work and geochemical analyses in order to understand its origin and relation to the main tonalite and granodiorite units. In addition we compiled and reviewed the about 400 chemical analyses of the Bergell intrusion available in the literature (many from unpublished Master and PhD theses). Secondly, we present high-precision U–Pb zircon measurements and intrusion pressures of four transition zone rocks, which allow us to better understand the magmatic evolution of this unit. Furthermore, we present a high precision age and intrusion pressures of the earliest Bergell plutonics deposited in the southern foreland basin (the Como molasse). Finally, the now available information allows reconstructing an intrusion history for the Bergell pluton.

2 The Bergell pluton

2.1 Geological setting

The Bergell pluton is a calc-alkaline intrusion occurring across the Swiss-Italian border in the Central Alps. The intrusion is build up by a granodioritic core unit of about 14×20 km in size that is mostly surrounded by a tonalite unit of typically 0.5–4 km width but which is absent in the northernmost part of the Bergell pluton (Berger 1996). In addition, the tonalite unit has a 30 km long westward tail, characterized by a strong penetrative deformation which is interpreted in the frame of a dextral movement later expressed in the Periadriatic Fault System (e.g. Berger et al. 1996; Davidson et al. 1996). The increasingly felsic nature of intrusives towards the center gives the Bergell the typical character of a normally zoned pluton, a feature found in many similar calc-alkaline bodies all over the world (e.g. Bateman and Chappell 1979; Halliday et al. 1980; Zorpi et al. 1989). Minor amounts of hornblendites, hbl-gabbros, diorites, qtz-diorites, aplites and pegmatites can also be observed (Reusser 1987; Diethelm 1989).

Al-in-hornblende geobarometry of tonalite samples have demonstrated an increase in hornblende crystallization pressures from 5 kbar at the eastern boundary with the Malenco serpentinite to 7.5 kbar in the western end of the tail of the tonalite unit near Bellinzona (Reusser 1987). Moreover the pluton displays a marked axial plunge of $\sim 25°$ at the eastern contact (Berger and Gieré 1995). These two features suggest that the Bergell intrusive body suffered a post-emplacement tilting, showing deeper levels in the west and shallower levels in the east.

Differences between the eastern and the western margin are also recognized in the contact metamorphism, directly observable only in the east, where the intrusion forms a contact aureole within the upper greenschist facies serpentinites of Val Malenco (Trommsdorff and Evans 1972, 1977; Trommsdorff and Connolly 1996). In the northwest, the intrusion has led to an increase in partial melting in the adjacent amphibolite-facies gneisses and pelites, which is manifested in back-veining of granitic material into the intrusion (Galli et al. 2013). In this northwestern area, the Bergell pluton intrudes the Gruf Complex (see Figs. 1a, 2) for which Alpine metamorphic conditions of 720–740 °C, 7–7.5 kbar (Galli et al. 2011) and Permian ultra-high temperature granulite facies conditions (up to 950 °C; Galli et al. 2012) were inferred. In contrast, no contact metamorphism has been described around the western tail of the tonalite unit, which intruded into the mostly gneissic Bellinzona-Dascio Zone that was at upper amphibolite facies conditions (700–750 °C, Burri et al. 2005). Nevertheless, such contact features may have been obliterated by the

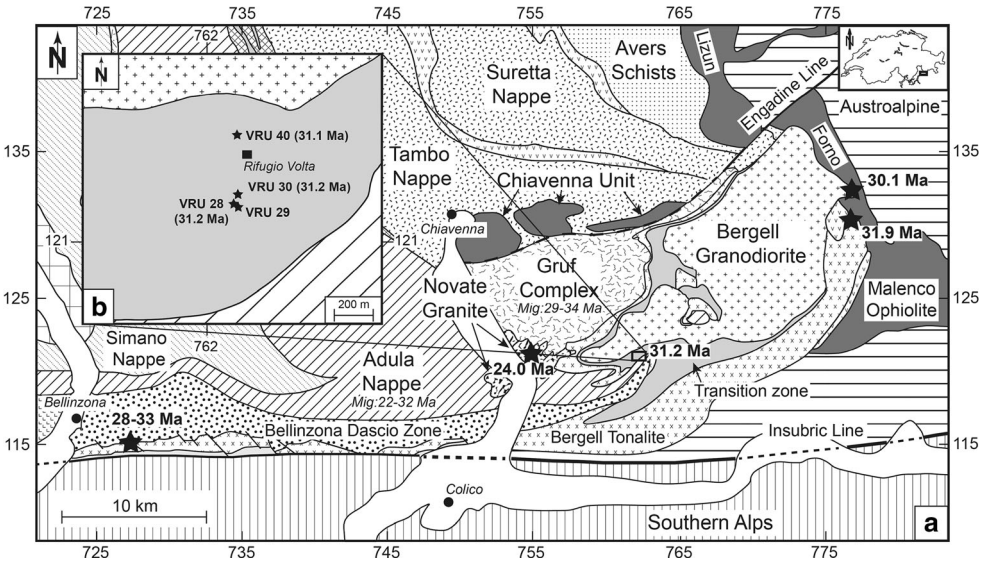

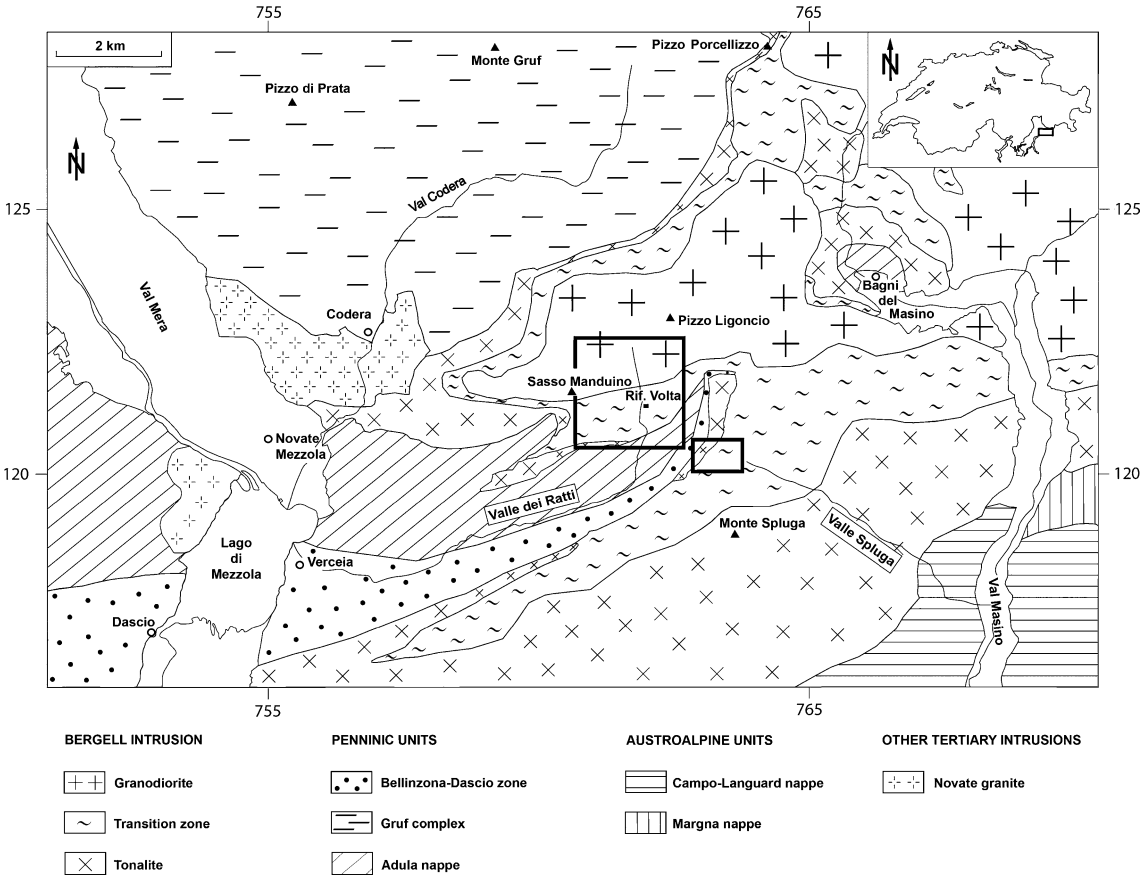

Fig. 1 **a** Schematic geological-tectonic map of the Central Alps (modified after Trommsdorff and Nievergelt 1983). *Black stars* represent locations of literature dated samples for the Tertiary intrusions (Bergell and Novate). For the Gruf complex and the Adula-Cima Lunga Nappe the age of migmatization is also given. **b** Transition zone in upper Valle dei Ratti around Rifugio Volta (Province of Sondrio, Italy). *Black stars* represent samples dated in this study

Fig. 2 Tectono-geological sketch (modified after Berger 1996) showing the sampling areas in upper Valle dei Ratti and in Valle Spluga

intensive syn- and post-intrusive deformation of the western tail.

The roof of the Bergell intrusion is nowadays completely eroded and only the mid to deeper parts are preserved (Reusser 1987; Davidson et al. 1996). The rocks that potentially represent this roof are the stratigraphically first occurrences of Bergell boulders deposited ~25 Myr ago (Giger and Hurford 1989; Bernoulli et al. 1993) in the southern foreland basin, i.e. in the Como molasse.

Tectonically the Bergell pluton is related in the south to the Insubric Line, a dextral segment of the 700 km long Periadriatic Fault System. Its deep precursor (Berger et al. 1996) presumably played a fundamental role in channeling the magma from its mantle source region (von Blanckenburg et al. 1992) into the crust (Berger et al. 1996; Rosenberg 2004; Galli et al. 2013). In the north, the Bergell intrusion reaches the NE–SW striking Engadine sinistral strike-slip fault, which contributed to the rotation of the batholith towards the north (Berger and Gieré 1995).

A peculiar feature of the Bergell intrusion, a subduction related calc-alkaline batholith, is that it is not located in the overriding plate, i.e. in the southern Alps of the Alpine subduction system (as are the Adamello and the Miagliano intrusions) but in the subducting continental northern plate. Von Blanckenburg et al. (1992) demonstrated that the source for the magma was an enriched sub-continental mantle undergoing decompression melting. This was then related to decompression melting in the aftermath of the slab break off (Davies and von Blanckenburg 1995; von Blanckenburg and Davies 1995) that led to the disappearance of the oceanic crust previously constituting the Thethys.

2.2 Timing

Hitherto, only three samples of the Bergell intrusion have been precision dated (Fig. 1a). U–Pb dating (von Blanckenburg 1992) performed on the two classic main units of the Bergell pluton yielded intrusion ages of 31.89 ± 0.09 Ma (U–Pb in zircon) for the tonalite unit and of 30.13 ± 0.17 (U–Pb in sphene and allanite) for the granodiorite unit. Nevertheless, U–Th–Pb isotope measurements on accessory minerals (zircon, titanite and allanite) indicate that a much longer crystallization history, spanning from 33 to 28 Ma has occurred at least in parts of the tonalite unit (Oberli et al. 2004). More recently, Gregory et al. (2009), applying the SHRIMP technique to allanite cores of magmatic epidote in a Bergell gabbro, obtained a Th–Pb intrusive age of 32.4 ± 0.4 Ma.

2.3 The tonalite and granodiorite main units

The main tonalite is composed of plagioclase, quartz, hornblende, biotite and minor amounts of epidote, K-feldspar and titanite ± magnetite or ilmenite. Magmatic epidote (often with allanite cores) is ubiquitous throughout the entire tonalite unit and had already been described by Cornelius (1915). Although the mineral assemblage remains the same over the almost 60 km E–W extension of the tonalite unit, different phenotypes of tonalite are observed (Reusser 1987). These range from hornblende-phyric with leucocratic minerals mainly in the interstices to plagioclase-phyric with xenomorphic hornblende. Together with a range in chemical composition that spans from gabbroic to granodioritc (53–68 wt% SiO_2, see discussion below), the tonalite unit must be regarded as a heterogeneous unit composed of a multitude of individual bodies. Nevertheless, the main minerals remain amphibole + plagioclase + biotite ± epidote + quartz and hence the classic tonalite unit may well be mapped as a single super-unit.

The granodiorite of the main unit is composed of plagioclase, quartz, biotite, minor hornblende (typically less than 10 vol%) and the distinctive K-feldspar megacrystals, which can reach 10 cm in size. Accessories include magmatic epidote with or without allanite cores. At its margins the granodiorite is characterized by magmatic fabrics distinguished by a preferred orientation of the K-feldspar megacrysts (e.g. Davidson et al. 1996). The main granodiorite unit is mostly massive and more homogeneous than the main tonalite unit. Nevertheless, SiO_2-concentrations span from 60–75 wt%, again mostly the result of a variation in mineral modes. The granodiorite contains blocks of the main tonalite body up to hundred meters in size (e.g. Reusser 1987) in accordance with the relative intrusion ages of the two main units.

3 Field and thin section observations

3.1 The transition zone in Valle dei Ratti

In the studied area, around Rifugio Volta (Province of Sondrio, Italy; Figs. 1a, b, 2), the transition zone is 500–800 m wide and characterized by a parallel, alternating pattern of different granodiorites and tonalites with a general WSW-ENE strike. The area is mostly polished by glaciers providing optimal outcrops for a several km wide profile reaching from the granodiorite unit in the north through the transition zone to the migmatitic gneisses of the Adula nappe and Bellinzona-Dascio Zone in the south (Moticska 1970). These parallel features are not observed in upper Val Codera, ~4 km to the north, where the transition zone is composed of small intrusives that lack a dominant foliation. The gneisses are wedged between the Bergell granodiorite and transition zone units to the north and a band of the main tonalite unit and further transition zone intrusives to the south. For most of its extension, the transition zone is located in between the main tonalite and granodiorite units. Nevertheless, in Valle dei Ratti the transition zone is also in direct contact with the country rocks (Fig. 1a, b).

The granodiorites and tonalites of the transition zone and of the main units contain mafic enclaves interpreted as magma mingling (Moticska 1970) and are cut by numerous

leucocratic granite dykes. These granitic dykes are mostly peraluminous with sometimes abundant muscovite ± garnet and also occasional beryl. Nevertheless, other dykes in the transition zone have only macroscopic biotite in addition to feldspars and quartz. From field evidence alone, it is not possible to distinguish whether individual aplite and pegmatite dykes represent late differentiates of the Bergell intrusion or minimum melts from the surrounding migmatitic gneiss units (where such dykes are common).

The transition zone tonalites consist of mesocratic, coarse-grained rocks with macroscopically visible plagioclase, quartz, amphibole (to >1 cm), biotite and some epidote. In the field, a second type of tonalite is distinguished by large K-feldspars (4–5 cm). Locally more melanocratic and leucocratic tonalite varieties can also be mapped.

The granodiorites are subdivided in a type characterized by K-feldspar megacrysts of typically 2–5 cm size and relatively little (<2 vol%) amphibole, an amphibole-rich (5 vol%) granodiorite (where amphiboles may reach cm-size) with large K-feldspars and an equigranular granodiorite characterized by equigranular K-feldspar and amphibole. The mineral assemblages for these granodiorites are the same as for the tonalites with the addition of abundant K-feldspar, showing sometimes typical Carlsbad twinning. In all granodiorites and tonalites few mm-sized titanite grains can be found.

Evidence for magmatic flow and mutual intrusive relations between tonalites and granodiorites are common in the transition zone. In the tonalites, magmatic flow features are schlieren with different sizes, ranging from a few decimeters up to 2 m and a preferred orientation of hornblendes (see also Davidson et al. 1996). The schlieren are composed of lenticular or flame-like diffuse concentrations of mafic minerals (commonly biotite and amphibole). In the granodiorites compositional banding (see Fig. 3a, b), preferred orientation of K-feldspars (see also Davidson et al. 1996), local accumulation of K-feldspars (see Fig. 3c) and schlieren (Fig. 3d) are observed. The compositional banding can be described as an alternating pattern of leucocratic and melanocratic bands, which thickness ranges from few cm to ~60 cm. The melanocratic bands are enriched in biotite and amphibole but sometimes also display an apparent enrichment in K-feldspar porphyroclasts. These latter are similar in size to those observed in the K-feldspar rich tonalite (4–5 cm) and often they are oriented parallel to the melanocratic bands. The leucocratic bands also show K-feldspar porphyroclasts but due to the lighter color of the matrix it is difficult to infer if the modal proportion of the porphyroclasts is really lower than in the melanocratic bands. On a microscopic scale, textures are dominated by subsolidus deformation and re-equilibration such as kink-bands, subgrain recrystallization and lobate grain boundaries. The majority of the foliations measured in the granodiorites and tonalites of the transition zone trend NE-SW [average: 076SE57 (strike, dip)], subparallel to the foliations measured in the gneisses of the Adula nappe to the south [average: 062SE61 (strike, dip)].

The mafic enclaves are constituted by amphibole, biotite, plagioclase, epidote, some quartz and occasionally K-feldspar. Most mafic enclaves occur as elongated and rounded, fine-grained ellipsoids of 10–50 cm maximum length, although some have a more rectangular shape. Many of the enclaves display highly irregular and deformed contours, suggesting that they were still partially molten when transported by the magma flow (see Fig. 3e).

Aplites consist of feldspars, quartz, garnet and some biotite, whereas pegmatites contain feldspars, quartz, small and rounded garnets, muscovite and rarely beryl. The leucocratic dykes intrude the rocks of the Bergell batholith but also the contiguous paragneisses of the Adula nappe and Bellinzona-Dascio Zone and have thicknesses ranging from few cm up to 1 m. The dykes show mutual intersections, irregular edges (Fig. 3f), and bifurcations (Fig. 3g). Some dykes have pegmatitic centers and aplitic borders, a feature that may stem from cooling from the dyke margins or fluid-saturation resulting from partial crystallization at the borders. The dykes generally strike E–W, similar to the granodiorites and tonalites, but they dip with 20°–70° northward and crosscut the southward dipping foliation of the granodiorites and tonalites. In addition, occasional steep (>70°–80°), N–S striking dykes are observed.

The main Bergell granodiorite unit north of the transition zone differs from the granodiorites of the transition zone by containing larger and a higher amount of K-feldspar megacrysts, which average size is ~7 to 8 cm (against max. 4–5 cm in the transition zone). Another distinctive characteristic of the main Bergell granodiorite is its massive appearance and a general lack of magmatic flow features such as schlieren or composite banding. Based on these features, a contact between the two rocks could be mapped, but this contact is gradational over a few meters, probably due to the development of a marginal facies within the main Bergell granodiorite.

The main tonalite unit is coarse-grained and composed mainly of plagioclase, elongated hornblende (up to 1 cm), quartz, biotite, epidote and some titanite. In the main tonalite, some minor quartz-diorite and abundant mafic enclaves are observed. The qtz-diorites form m-scale lenses of coarse-grained melanocratic rocks composed of plagioclase, hornblende, biotite, minor quartz and epidote.

In the investigated profile, the generally E–W striking migmatitic gneisses are in a direct concordant contact with the transition zone intrusives. These gneisses are

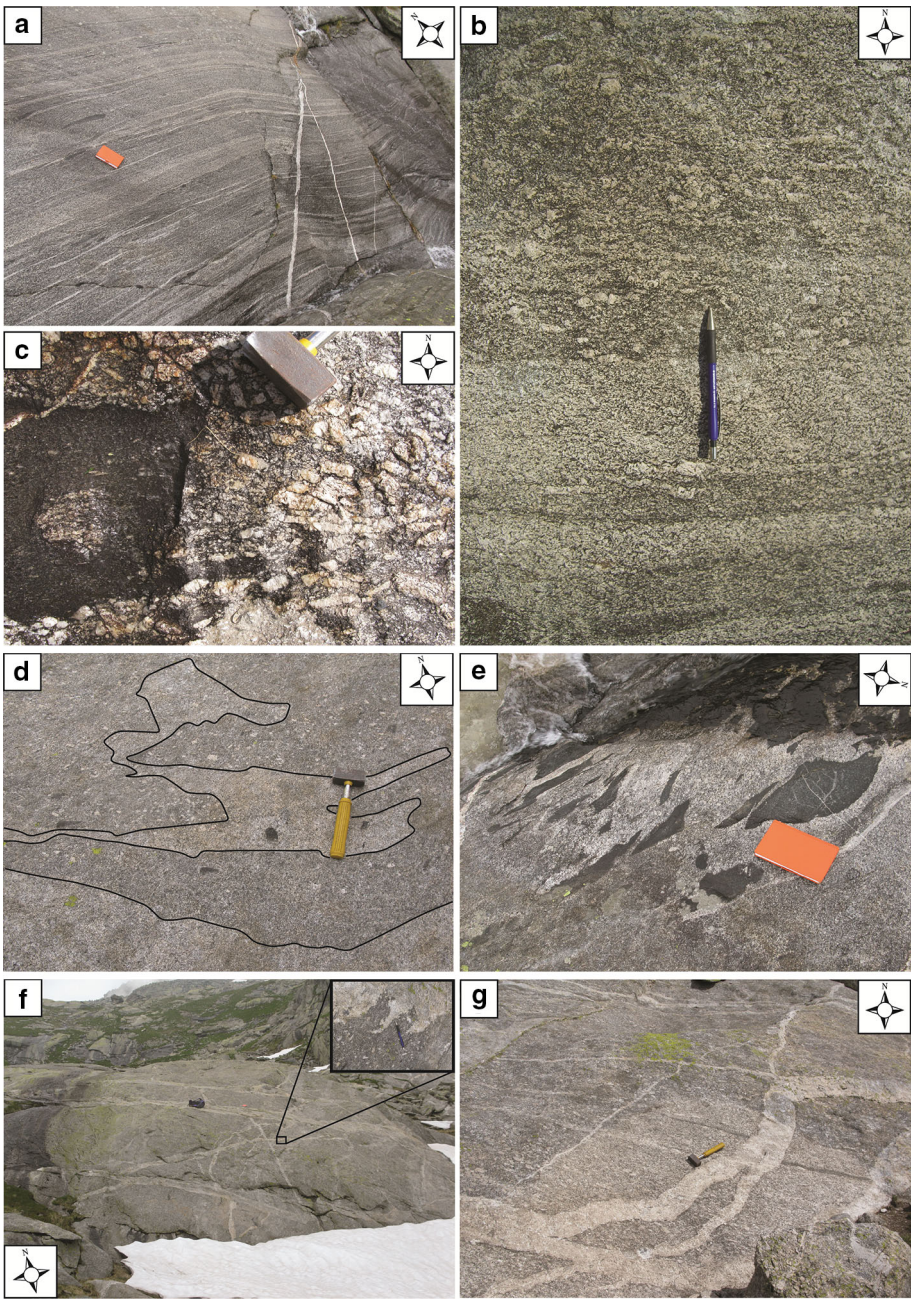

Fig. 3 **a** Parallel compositional banding in the transition zone. **b** Detail picture of the compositional banding (same as in **a**) showing enrichment of K-feldspar megacrystals in the mafic intrusives. **c** Accumulation of K-feldspars near a mafic enclave. **d** Characteristic appearance of schlieren (*darker* part outlined in *black*). **e** Mafic enclaves probably deformed during a still partial molten state. **f** Aplitic and pegmatitic dykes in the typical Bergell granodiorite and in detail the irregular edge of one of these dykes. **g** Bifurcation in pegmatitic dyke

predominantly composed of feldspar, quartz, biotite, muscovite and garnet. Their migmatization is overprinted by a nearly isoclinal folding with E–W trending fold axis. Dykes that crosscut these folds are observed. The gneisses of Valle dei Ratti may belong to two different units: the Bellinzona-Dascio zone or the Adula nappe (see also Moticska 1970; Schmid et al. 1996; Stucki 2001).

3.2 Bergell intrusives sedimented in the Como molasse

These conglomerates containing typically 10–20 cm but up to 60 cm large boulders interpreted as Bergell intrusives were described by several authors (e.g. Gulson and Krogh 1973; Wagner et al. 1977, 1979; Jäger and Hantke 1984; Giger and Hurford 1989; Oschidari and Ziegler 1992; Bernoulli et al. 1993; Fox et al. 2014). In this study, eight different outcrops in the S of Chiasso, still on Swiss territory, were surveyed. In the observed conglomerates, tonalites are typically 40 but also up to 60 vol% of the boulders, while granodiorites are about 20–30 vol%. While most tonalites are fresh, most granodiorites are weathered. Nevertheless, four fresh granodiorite and six tonalite samples were collected. The mineralogical description of these rocks is very similar to those of the two main units as

described above except for a complete absence of magmatic epidote; the tonalites are hornblende-phyric and the granodiorites contain K-feldspar of up to 7 cm.

4 Analytical methods

4.1 Major and trace element compositions

Bulk rock compositions were determined by X-ray fluorescence (XRF) analysis of glass pellets prepared using Li-tetraborate ($Li_2B_4O_7$) at the Institute for Geochemistry and Petrology (IGP), ETH Zurich. Trace elements concentrations for selected samples were measured at IGP (ETH Zurich) with Laser Ablation Inductively Coupled Plasma-Mass Spectrometry (LA-ICPMS) on the same glass pellets. The aperture of the laser beam was 90 μm for standard and samples and 40 μm for the blank. The NIST 610 standard was measured in order to estimate the reproducibility of the analyses (Günther et al. 2001). Trace element concentrations in zircons were also measured with LA-ICPMS using a beam size of 60 μm for the zircon crystals, 90 μm for the standard (NIST 610) and 40 μm for the blank.

4.2 U–Pb zircon dating technique

Samples were crushed and sieved in order to obtain a fraction with grain size between 100 and 300 μm, from which the magnetic minerals were separated. Zircons were then extracted using standard heavy liquids (methyl iodide and Clerici solution) followed by hand picking. According to the procedures of Mattinson (2005) and von Quadt et al. (2011), zircons were first annealed at 850 °C for 48 h, subsequently leached with concentrated HF at 180 °C for 12 h and finally washed several times with pure water, then with acetone and then with HCl. The chemically abraded zircons were individually weighed and inserted in Teflon® bombs with a mixture of concentrated HF and HNO_3 and a double-spike solution ($^{202,205}Pb/^{233,235}U$). Then each Teflon® bomb was jacketed in a steel cylinder and put in an oven at 205 °C for 6 days until zircons were completely dissolved. An anion-exchange resin technique allowed recovering U and Pb from the solutions. The U and Pb isotopic compositions were then measured with a ThermoFisher (TRITON plus) TIMS at IGP (ETH Zurich). Decay constants of Steiger and Jäger (1977) were used for age calculations and corrections for common Pb were made according to the values of Stacey and Kramers (1975).

4.3 Electron microprobe analysis

Electron microprobe analyses were performed at ETH Zurich using a JEOL JXA-8200 electron microprobe equipped with 5 WDS crystal spectrometers. Analyses were carried out on polished thin sections using a beam current of 20 nA and an accelerating voltage of 15 kV. Natural and synthetic standards were used for calibration of the instrument. Measurements were conducted with measuring times of 10 s for Na and K and 20 s for the other elements on the peaks and 10 s on the background position.

5 Whole rock chemistry of the transition zone intrusives

Whole rock analyses of samples collected in Valle dei Ratti and in Valle Spluga (Fig. 2) are listed in Table 1. In the AFM diagram (Fig. 4a), the transition zone samples follow a calc-alkaline trend congruent to that of the Bergell main granodiorite and tonalite units (see below). According to their leucocratic nature, the aplitic and pegmatitic dykes are almost in the $Na_2O + K_2O$-corner of the AFM diagram. Normative albite, anorthite and K-feldspar contents yield tonalitic to granodioritic to quartz-monzonitic compositions (Fig. 4b); only the aplitic and pegmatitic dykes fall into the granite field. The CIPW-norm leads to an overestimation of the orthoclase component, as the potassium stored in biotite is also attributed to orthoclase. Consequently, some tonalites plot into the granodiorite field. The rocks of the transition zone span a range from 49 (mafic enclaves) to 76 wt% SiO_2 (aplitic and pegmatitic dykes). The measured granodiorites, as defined by their phenotype, span a range of SiO_2-concentrations from 54 to 71 wt%. The lower end of this Si-range can be explained by biotite and also hornblende accumulation in combination with K-feldspar fractionation and a relatively increased abundance of oxides (max. 3 vol%). On the other hand, the measured tonalites range only from 62 to 65 wt% SiO_2. As to be expected, major element Harker diagrams (Fig. 5a–j) display negative trends with increasing differentiation except for Na_2O and K_2O, which increase with differentiation. On the other hand, most transition zone samples, i.e. the mafic enclaves and the different types of tonalite and granodiorite have a constant X_{Mg} near 0.5, and only the aplites and pegmatites have an $X_{Mg} < 0.2$.

Trace elements for the rocks of the transition zone plotted against SiO_2 (Fig. 6a–f) display a negative trend for Co, Sc, Zr and Sr, whereas for Rb the trend is positive and for Ba is not possible to determine any particular correlation.

N-MORB (Sun and McDonough 1989) normalized trace element patterns (Fig. 7a–d) display a significant enrichment in the large ion light elements (LILE, such as Cs, Rb, K and Ba), a strong negative anomaly of Nb and Ta and a weak negative anomaly of Zr, Hf, and Ti as typical for calc-alkaline series (Best 2003). A strong positive anomaly

Table 1 Selected bulk rock compositions

	Tonalite TZ		K-fsp rich tonalite TZ		Equigranular granodiorite TZ		Hbl rich granodiorite TZ		Granodiorite TZ	
	VRU 9	VRU 33	VRU 28	VRU 30	VRU 8	VRU 26	VRU 1A	VRU 31	VRU 29	VRU 40
Longitude	761′525	764′012	762′112	762′108	761′476	762′134	762′290	764′017	762′112	762′137
Latitude	120′918	120′751	121′181	121′165	121′011	121′303	121′424	120′634	121′181	121′425
SiO_2	61.95	64.47	64.03	64.01	67.29	66.40	58.05	63.69	59.10	64.29
TiO_2	0.63	0.55	0.56	0.54	0.42	0.48	0.67	0.57	0.59	0.54
Al_2O_3	16.39	15.79	16.60	16.19	15.80	16.17	18.04	16.62	19.09	17.36
Fe_2O_3	5.48	4.79	4.81	4.53	3.65	4.03	5.82	4.44	4.38	4.03
MnO	0.10	0.10	0.08	0.10	0.06	0.08	0.12	0.09	0.08	0.06
MgO	2.77	2.41	2.36	2.37	1.83	2.09	3.00	2.21	2.16	1.93
CaO	5.44	4.68	4.57	4.61	3.60	3.89	5.28	4.31	3.95	3.81
Na_2O	3.39	3.11	3.84	3.30	3.69	3.86	3.72	3.20	3.67	3.95
K_2O	2.46	3.37	2.08	2.66	2.25	2.16	4.05	4.13	5.60	3.47
P_2O_5	0.22	0.18	0.24	0.21	0.18	0.19	0.47	0.25	0.57	0.27
LOI	0.79	0.62	0.62	0.74	0.55	0.57	0.70	0.65	0.75	0.56
Total	99.63	100.10	99.79	99.26	99.32	99.95	99.93	100.16	99.98	100.28
Sc	17.47	15.05	16.19	13.07	12.94	11.76	20.33	10.17	8.33	3.32
V	119.59	112.24	109.98	116.43	71.03	100.34	120.49	109.78	93.16	77.95
Cr	18.78	18.91	19.91	25.20	19.14	23.64	30.85	21.28	22.91	33.02
Co	12.15	10.78	10.73	12.20	8.43	9.76	13.25	10.60	9.44	7.76
Ni	5.85	6.45	7.61	12.07	9.77	11.86	11.09	8.54	12.89	11.15
Zn	31.48	35.50	40.49	40.55	30.41	30.78	41.68	36.41	50.33	37.97
Ga	14.29	14.34	16.61	15.73	16.00	15.56	18.78	15.90	20.19	17.45
Rb	102.69	118.70	105.74	106.68	99.72	136.37	158.68	159.69	200.60	152.09
Sr	437.84	309.08	355.57	303.30	270.18	256.27	487.16	304.77	394.48	274.86
Y	21.49	21.90	15.92	21.15	15.36	16.81	37.45	17.45	17.91	10.21
Zr	173.59	138.30	180.15	132.04	140.56	148.33	286.74	164.39	232.47	198.21
Nb	11.69	12.34	14.91	11.46	8.99	15.40	18.80	10.68	13.76	14.69
Cs	2.51	2.84	3.08	2.64	2.23	7.51	3.92	3.38	4.39	4.01
Ba	682.80	891.01	360.61	1106.78	435.86	482.75	1744.91	1126.95	2273.85	692.74
La	29.92	13.57	27.69	24.08	30.79	20.72	52.76	30.71	26.11	40.35
Ce	51.40	27.55	51.96	48.67	54.25	42.44	101.51	60.91	54.02	72.46
Pr	5.93	3.55	5.68	5.45	6.19	4.61	11.96	6.35	5.86	7.91
Nd	23.75	15.76	21.47	20.97	23.63	19.55	47.71	23.16	22.05	27.18
Sm	4.21	4.41	4.96	4.86	4.47	4.68	9.58	4.38	5.31	4.11
Eu	1.15	1.01	0.77	1.20	0.73	0.71	1.47	1.07	1.28	0.95
Gd	4.31	4.25	4.08	4.44	4.02	3.33	8.57	3.72	4.39	2.91
Tb	0.64	0.73	0.55	0.72	0.50	0.48	1.12	0.57	0.73	0.34
Dy	3.69	5.01	3.22	5.08	2.93	2.92	6.58	3.99	4.72	1.91
Ho	0.67	0.78	0.52	0.81	0.56	0.50	1.28	0.70	0.71	0.34
Er	2.29	2.18	1.61	2.43	1.55	1.77	3.34	1.85	1.85	0.98
Tm	0.28	0.35	0.21	0.38	0.18	0.23	0.50	0.25	0.28	0.14
Yb	1.89	2.35	1.31	1.68	1.22	1.47	3.23	1.72	1.67	1.01
Lu	0.32	0.36	0.22	0.37	0.14	0.22	0.51	0.32	0.22	0.14
Hf	4.51	4.31	5.32	5.16	3.91	4.86	7.19	5.98	8.30	5.96
Ta	0.96	1.99	1.03	1.05	0.65	1.98	2.38	1.26	1.21	1.40
Pb	13.29	24.30	16.42	21.77	14.33	14.22	21.07	31.99	36.27	21.17
Th	17.07	9.91	13.32	12.91	13.84	20.94	25.29	26.52	12.18	18.44
U	2.49	3.57	2.64	2.35	1.84	9.90	5.35	4.60	3.70	6.67

Table 1 continued

	Mafic enclave	Aplite	Qz-diorite		Granodiorite main unit	Tonalite Como molasse		Granodiorite Como molasse	
	VRU 1B	VRU 11	VRT 1	VRT 2	VRG 1	CMB-4	CMB-9	CMB-5	CMB-15
Longitude	762′290	761′891	763′348	763′382	762′099	723′092	721′448	721′396	723′275
Latitude	121′424	120′757	120′642	120′691	122′591	76′280	76′466	76′560	76′035
SiO_2	49.13	74.84	47.90	53.19	69.06	59.32	62.61	65.02	66.04
TiO_2	1.17	0.01	1.27	0.91	0.36	0.70	0.58	0.18	0.44
Al_2O_3	18.00	14.36	19.44	18.43	15.54	17.34	16.01	17.01	15.99
Fe_2O_3	9.35	0.70	10.32	8.07	2.87	6.50	5.10	2.09	3.52
MnO	0.22	0.18	0.16	0.14	0.05	0.11	0.09	0.04	0.06
MgO	5.48	0.03	5.28	4.30	1.12	3.45	2.64	1.09	1.91
CaO	8.06	0.53	9.51	8.01	2.75	6.41	4.72	2.18	3.50
Na_2O	3.96	4.51	2.99	3.16	3.60	3.21	2.84	2.58	3.59
K_2O	2.62	3.88	1.95	1.92	4.01	2.15	3.88	8.36	3.67
P_2O_5	1.05	0.10	0.37	0.33	0.21	0.16	0.18	0.13	0.26
LOI	0.94	0.44	0.80	0.85	0.51	0.98	1.03	0.85	0.93
Total	100.00	99.57	100.00	99.31	100.08	100.33	99.69	99.53	99.90
Sc	31.84	–	33	23	5	19	16	14	8
V	218.88	3	287	219	40	167	123	40	70
Cr	61.58	1	21	30	10	18	50	57	35
Co	21.41	–	28	26	6	29	23	16	18
Ni	22.53	4	9	14	13	11	8	18	20
Zn	70.45	27	91	75	51	61	54	29	48
Ga	19.84	19	24	20	20	24	23	20	25
Rb	155.86	255	74	79	160	96	157	209	158
Sr	405.71	15	480	496	401	261	301	484	405
Y	53.01	10	51	38	20	26	21	15	16
Zr	342.77	31	201	208	236	167	154	96	192
Nb	27.79	13	11	10	8	8	8	5	11
Cs	4.83	–	–	–	–	–	–	–	–
Ba	498.34	10	725	849	774	419	1143	3200	916
La	30.30	8	17	8	34	4	–	27	30
Ce	85.39	–	72	65	76	48	45	67	66
Pr	12.44	–	–	–	–	–	–	–	–
Nd	56.12	3	29	26	30	24	23	30	30
Sm	12.61	–	–	–	–	–	–	–	–
Eu	2.70	–	–	–	–	–	–	–	–
Gd	11.30	–	–	–	–	–	–	–	–
Tb	1.54	–	–	–	–	–	–	–	–
Dy	9.21	–	–	–	–	–	–	–	–
Ho	1.66	–	–	–	–	–	–	–	–
Er	4.99	–	–	–	–	–	–	–	–
Tm	0.69	-	-	-	-	-	–	–	–
Yb	4.98	-	-	-	-	-	–	–	–
Lu	0.62	-	-	-	-	-	–	–	–
Hf	8.61	2	5	5	5	9	8	8	12
Ta	1.80	–	–	–	–	–	–	–	–
Pb	13.15	–	–	–	–	17	38	52	33
Th	14.64	1	4	3	18	3	10	12	17
U	7.36	11	13	11	13	1	3	3	3

Major elements are given in wt%, trace elements in ppm

TZ transition zone

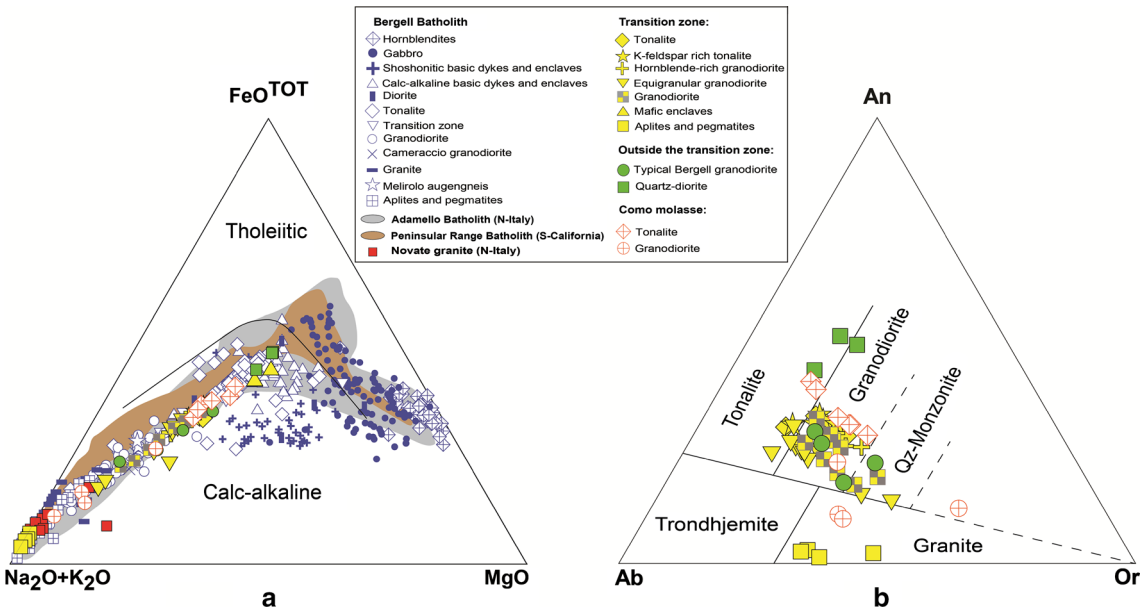

Fig. 4 **a** AFM diagram (Irvine and Baragar 1971). **b** Normative albite-anorthite-orthoclase classification scheme of silicic plutonic rocks (O'Connor 1965). Note that in the field, a classification as pheno-tonalite or pheno-granodiorite is based on appearance (mainly hornblende and K-feldspar megacrystals) and does not necessarily correspond to the classification based on geochemical criteria. Analyses are renormalized to 100 % on anhydrous basis

for Pb can be observed in all samples, but a relative positive anomaly for Sr is absent. A negative Eu anomaly indicates early fractionation of plagioclase from the melt which in turn may also explain the absence of the positive Sr-anomaly. REE patterns have negative slopes with $(Sm/La)_N$ ratios ranging of 0.10–0.40, and $(Lu/Gd)_N$ ratios of 0.28–0.70. The similar REE-patterns (and characteristic trace elements and trace element ratios) of the intermediate-acidic samples and the mafic enclaves of the transition zone are coherent with an origin from the same parental magma.

6 Hornblende geobarometry

Amphibole compositions have been measured in four transition zone rocks and in six boulders from the Como molasse in order to calculate Al-in-hornblende intrusion pressures (Hammarstrom and Zen 1986). In the transition zone, these samples are one average tonalite (VRU 9), two K-feldspar rich tonalites (VRU 28 and VRU 30) and one granodiorite (VRU 13), all bearing magmatic epidote and the full assemblage required for Al-in-hornblende barometry (Hammarstrom and Zen 1986; Schmidt 1992). The boulders in the Como molasse are five epidote-free tonalites (containing two oxide phases) and one granodiorite. In all samples, amphiboles are weakly zoned and rim compositions have been chosen to calculate intrusion pressures. The results are given in Table 2.

For the transition zone, pressures of 6.0–6.2 ± 0.7 kbar resulted, which fit smoothly with the compilation of Davidson et al. (1996, their Fig. 9) where the next nearest sample, less than 2 km to the east, yielded 6.7 kbar and two samples 4–6 km to the west gave intrusion pressures of 5.8–6.1 kbar. These latter three samples are from the main tonalite unit, resulting in the observation that an eventual uplift between the intrusion of the tonalite and transition zone units is within error of the barometric method (at least ±0.5 kbar, Schmidt 1992).

For the tonalite boulders of the Como molasse, we obtained intrusion pressures of 3.3–3.8 ± 0.6 kbar, yielding an average of 3.6 ± 0.8 kbar. The single granodiorite containing amphibole gave 4.0 ± 0.6 kbar. The latter is not much distinct from the lowest intrusion pressures of the Bergell granodiorite unit in its NE corner (4.5 kbar; Davidson et al. 1996), but the main granodiorite unit contains magmatic epidote while the boulders do not. Intrusion pressures in the epidote-bearing main tonalite unit do generally not decrease below 5.8 kbar and hence are much higher than those determined for the boulders deposited in the Como molasse. The significance of this finding will be discussed below.

7 Zircon dating

7.1 Analyzed samples

Four rock samples were collected along a 350 m profile inside the transition zone in Valle dei Ratti (100 m SW of Rifugio Volta; Fig. 1b). They comprise two different

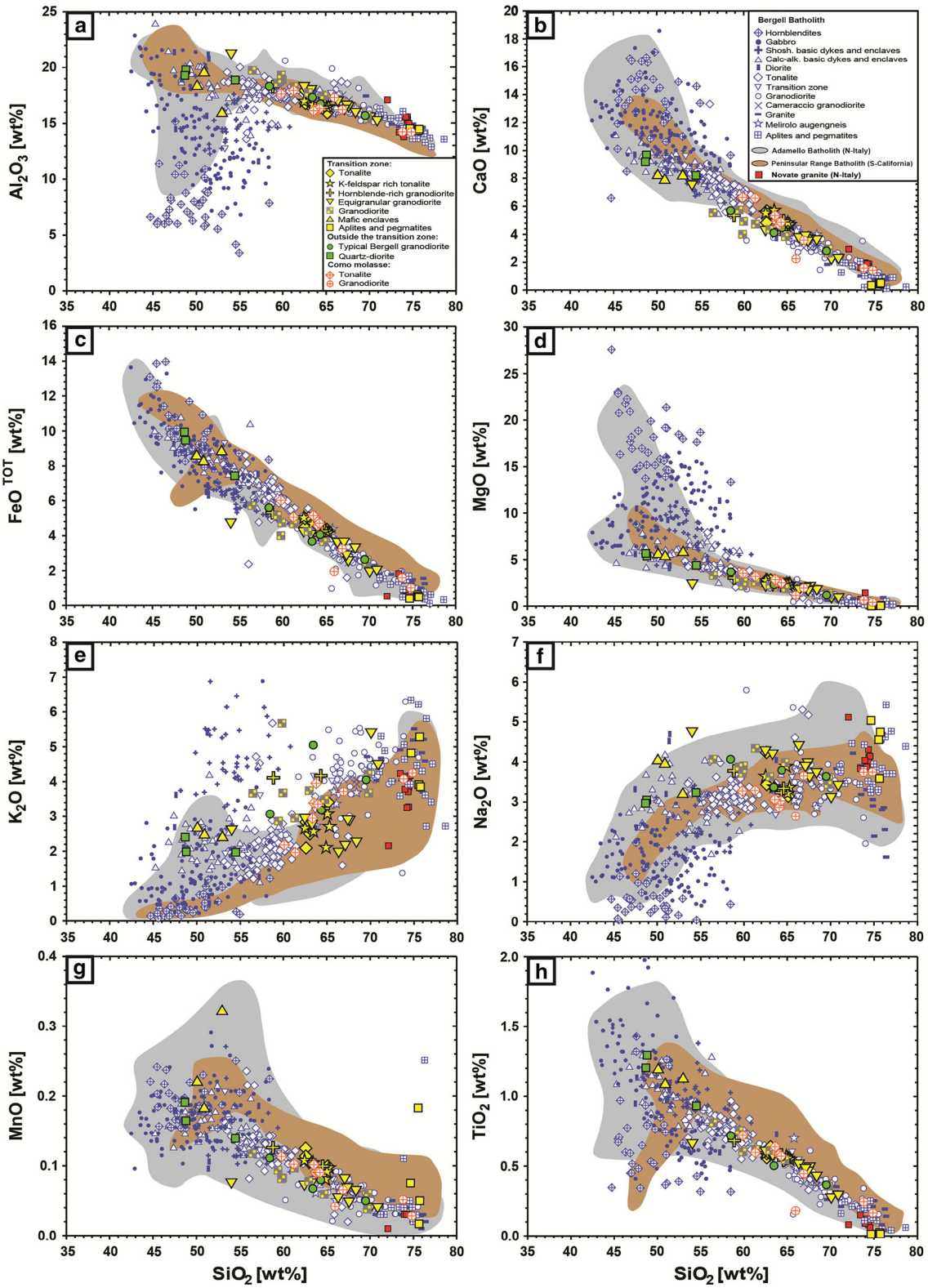

Fig. 5 Major elements vs. SiO_2 (*symbols* and *shaded areas* same as in Fig. 4). Analyses are renormalized to 100 % on anhydrous basis

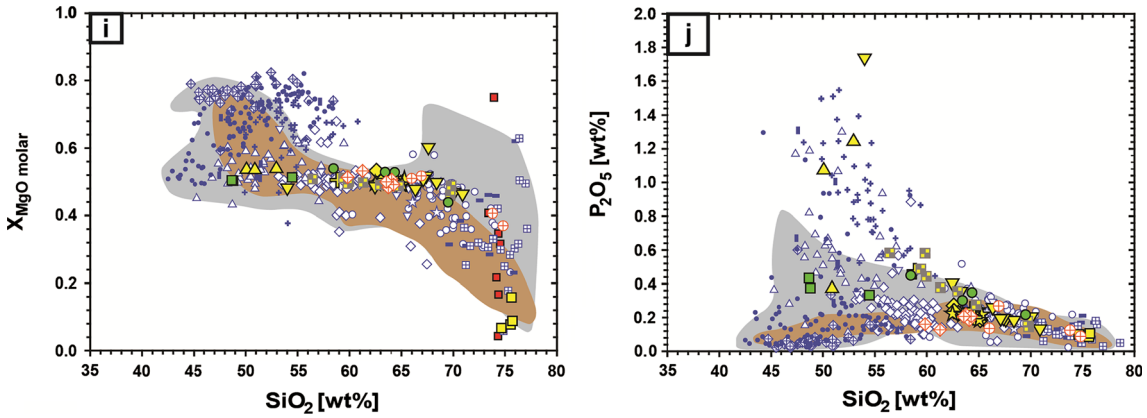

Fig. 5 continued

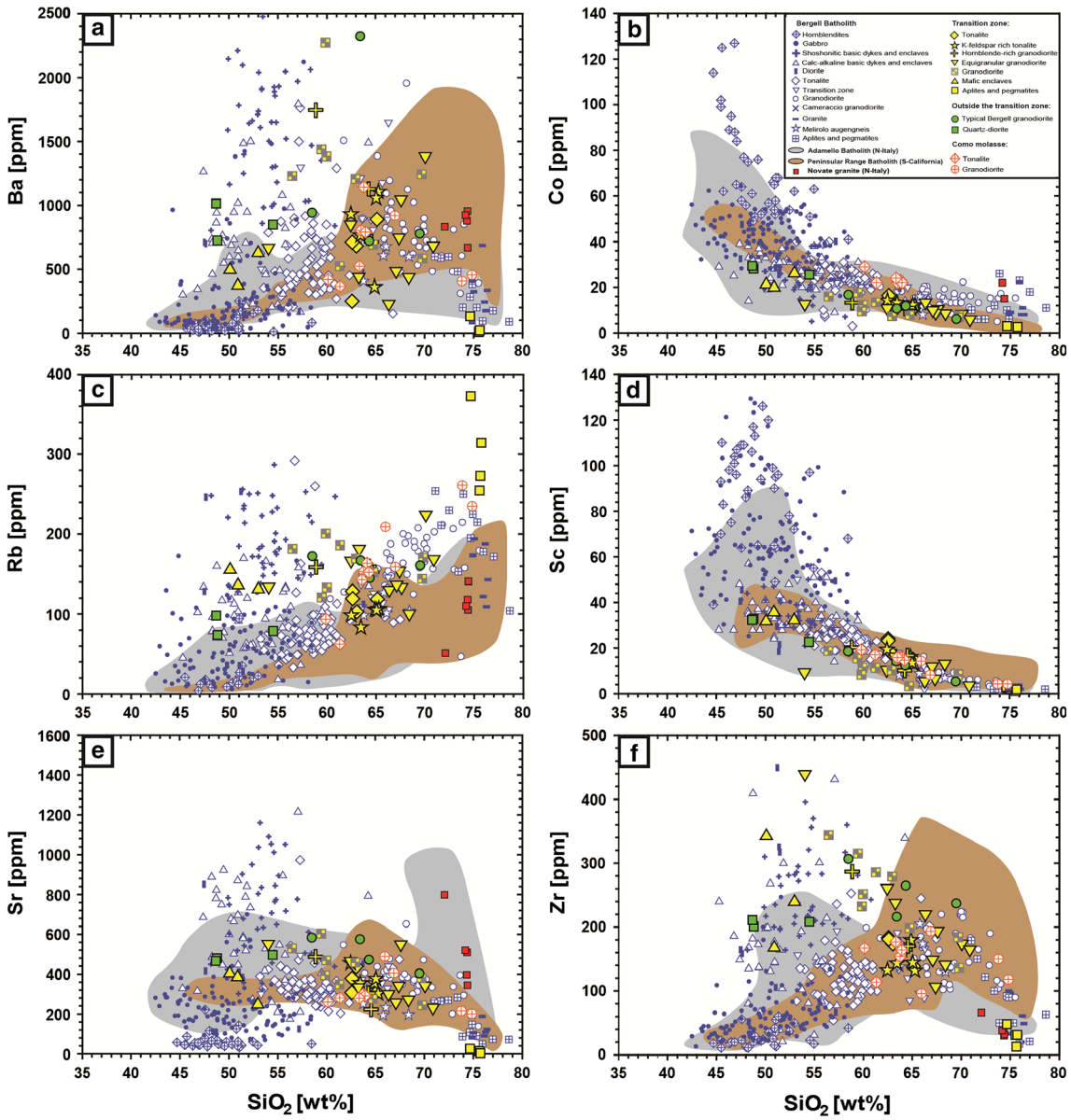

Fig. 6 Trace elements vs. SiO_2 (*symbols* and *shaded areas* same as in Fig. 4)

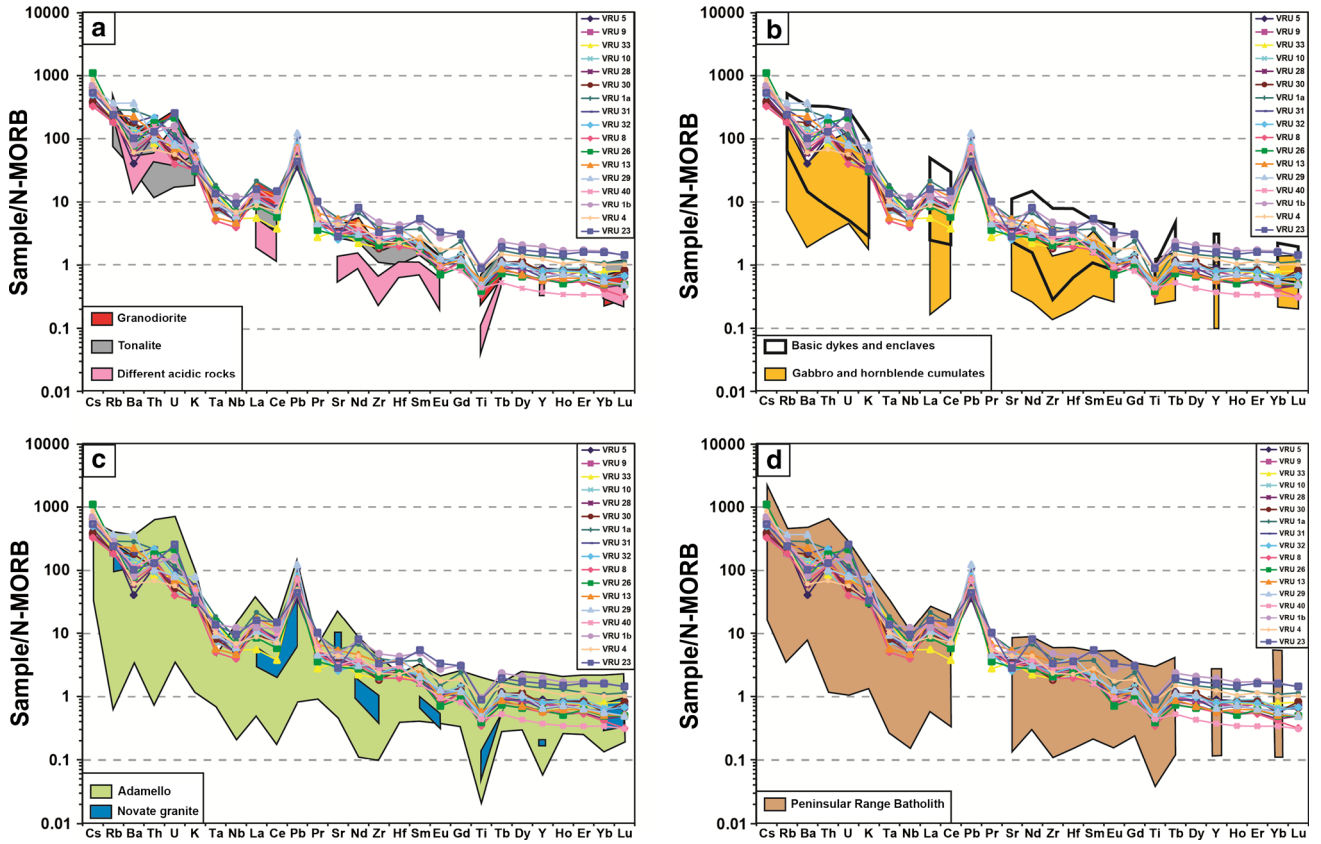

Fig. 7 Trace element patterns for the rocks of the transition zone normalized to N-MORB (Sun and McDonough 1989) compared to: **a** typical granodiorite, typical tonalite and other acidic rocks of the Bergell intrusion; **b** mafic dykes, enclaves and cumulates from the Bergell; **c** the adjacent S-type Novate granite and the compositional array of the Adamello batholith, and **d** the Peninsular Range batholith

Table 2 Al-in-hornblende geobarometry (rim analyses) for samples from the Bergell transition zone and the Como molasse

	Sample	Rock type	Al^{TOT} (apfu)	Pressure (kbar)	Depth (km)
Bergell transition zone	VRU 13	Granodiorite	1.94	6.2	22.8
	VRU 9	Tonalite	1.89	6.0	22.1
	VRU 28	K-fsp rich tonalite	1.90	6.0	22.1
	VRU 30	K-fsp rich tonalite	1.94	6.2	22.8
	Average tonalite transition zone		1.91 ± 0.03	6.1 ± 0.7	22.3 ± 1.8
Como molasse	CMB-15	Granodiorite	1.48	4.0	14.7
	CMB-4	Tonalite	1.37	3.5	12.9
	CMB-12	Tonalite	1.43	3.8	14.0
	CMB-9	Tonalite	1.40	3.7	13.6
	CMB-18	Tonalite	1.32	3.3	12.1
	CMB-6	Tonalite	1.39	3.6	13.2
	Average tonalite Como molasse		1.38 ± 0.04	3.6 ± 0.8	13.2 ± 2.6

granodiorites of the transition zone (VRU 29, Swiss grid coordinates: 762 112/121 181 and VRU 40, coordinates: 762 137/121 425) and two different K-feldspar rich tonalites (VRU 28, coordinates: 762 112/121 181 and VRU 30, coordinates: 762 108/121 165). The four units are between 0.5 and 2 m thick and VRU 28 and VRU 29 are from adjacent units, while VRU 30 is located 15 m further to the north, with several other granodiorite and tonalite units in between. VRU 40 is about 150 m to the north of the three other samples (Fig. 1b).

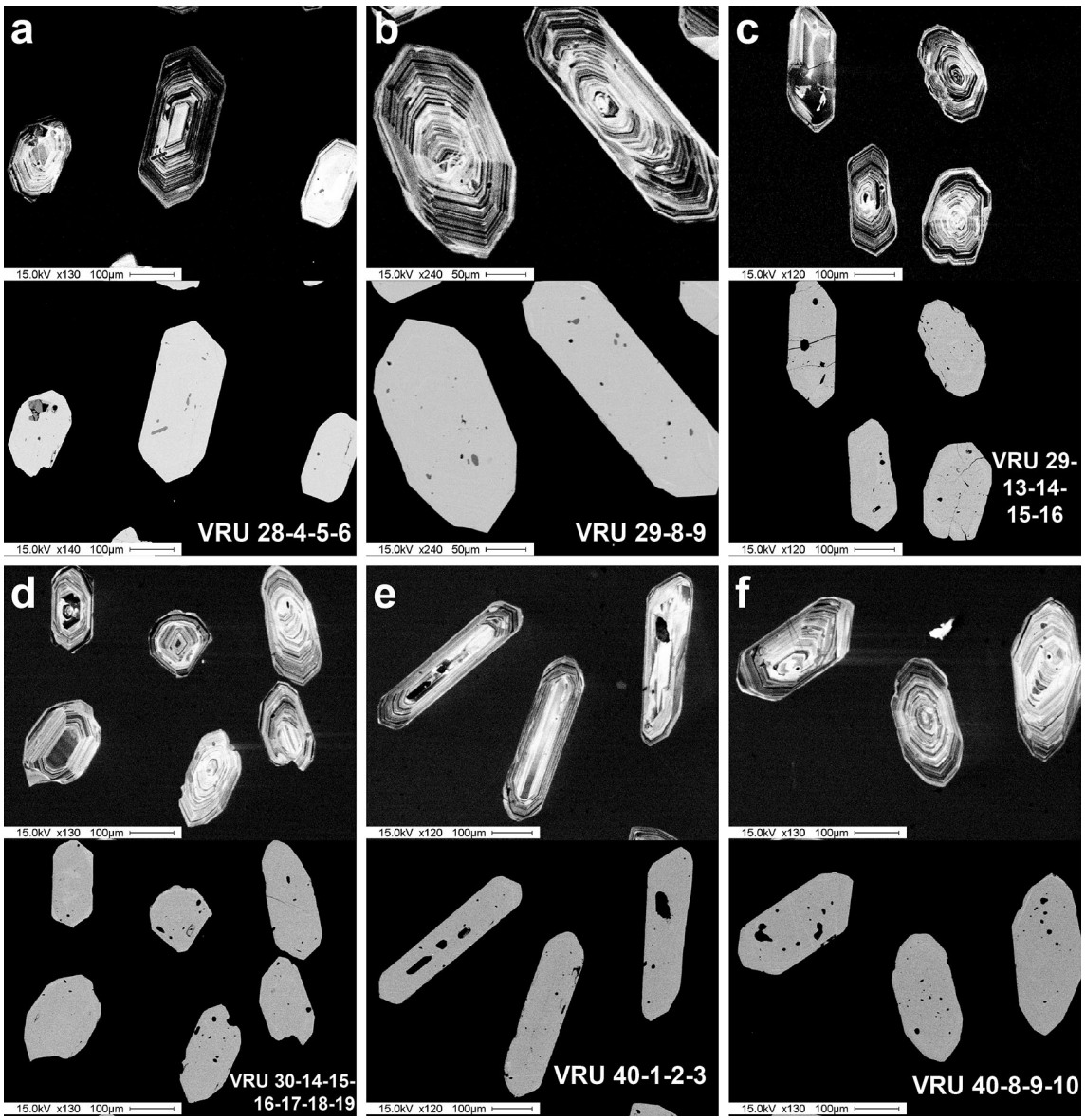

Fig. 8 Image pairs of zircons of the dated samples. For each pair, the top is a cathodoluminescence (CL) and bottom a back-scattered electron (BSE) image. Crystals display the typical oscillatory magmatic zoning

7.2 Characteristics of zircons

Under the optical microscope zircons can be subdivided into two groups. One group is transparent, while the second group is brownish in color. In both groups, however, most of the crystals are elongated (some showing the typical pyramidal shape and others display more rounded contours). This was emphasized after the analyses with cathodoluminescence (CL) and back scattered electrons (BSE; Fig. 8a–f), which also revealed a clear oscillating pattern zoning, typical for magmatic zircons, where no inherited cores could be observed. CL and BSE images also show that some zircons are multiply fractured (Fig. 8c), a feature that could have affected U–Pb loss or fluid-crystals interactions in the zircons.

7.3 REE chemistry

Zircon trace element analyses are compiled in Table 3. Normalized zircon trace element patterns (Fig. 9a) display enrichment relative to CI-chondrites (McDonough and Sun 1995), with exception for La and Pr in some zircons. The REE patterns are characterized by a positive Ce anomaly ($Ce_N/Ce^* = 1.35–128.12$, and 0.93–1.16 for bulk rock; $Ce^* = (La_N \cdot Pr_N)^{1/2}$), characteristic for magmatic zircons and due to the preferential incorporation of Ce^{4+} (instead

Table 3 LA-ICP-MS analyses of zircons from the dated samples

	K-fsp rich tonalite transition zone									
	VRU 28-2	VRU 28-3	VRU 28-5	VRU 28-10	VRU 28-13	VRU 30-2	VRU 30-6	VRU 30-11	VRU 30-15	VRU 30-17
P	1837	855	1219	1241	2082	984	489	1057	366	143
Ti	3.96	5.28	4.69	6.49	6.03	2.48	3.73	4.80	6.36	1.94
V	–	0.39	0.24	0.30	0.90	0.18	0.21	2.13	0.54	0.17
Mn	6.78	5.94	9.24	14.92	24.38	7.30	3.66	10.56	8.38	–
Rb	0.16	0.17	0.24	1.33	0.39	0.28	0.38	0.23	0.59	0.18
Sr	1.38	1.57	2.42	2.21	6.35	1.13	1.34	2.39	0.64	0.24
Y	649	614	676	329	583	994	530	779	1036	797
Zr	391954	409865	383571	445895	472647	369336	392583	436427	425625	309469
Nb	2.49	2.90	2.27	2.79	2.64	4.21	3.45	5.79	5.43	4.94
La	2.35	3.56	5.94	7.16	12.28	1.63	2.51	4.78	0.63	0.08
Ce	20.78	22.78	27.72	25.39	37.47	25.94	24.68	33.50	24.49	25.25
Pr	0.83	1.17	1.60	2.02	3.67	0.49	0.61	1.29	0.28	0.06
Nd	3.54	4.20	6.62	7.99	13.98	3.39	2.72	6.12	2.25	0.83
Sm	2.75	2.40	3.52	2.26	4.14	2.75	1.74	2.19	3.04	1.30
Eu	0.83	0.71	1.06	0.43	1.03	0.91	0.58	0.67	1.07	0.70
Gd	11.62	10.49	12.88	6.53	14.68	15.54	8.31	9.12	16.84	10.59
Tb	3.73	3.23	4.11	2.08	4.51	5.24	2.87	3.45	5.80	4.02
Dy	46.41	43.29	52.12	23.55	44.87	70.89	40.27	46.85	80.19	49.64
Ho	19.65	18.45	20.77	9.88	19.80	29.81	16.37	20.85	29.35	22.67
Er	103.11	102.38	108.40	58.66	113.23	163.90	91.24	122.97	181.69	112.83
Tm	22.90	22.43	24.98	13.87	25.01	38.55	20.24	30.35	39.18	30.31
Yb	278.3	263.4	284.9	151.0	254.8	428.2	226.3	367.7	445.3	324.7
Lu	61.67	57.32	60.28	33.75	53.92	94.51	47.92	82.84	90.67	82.59
Hf	7933	8764	8332	11042	10525	9315	9293	13105	12484	8042
Ta	0.93	1.10	1.01	1.32	0.79	2.29	1.81	3.49	2.73	2.40
Pb	11.86	10.35	12.90	9.92	8.97	34.91	18.72	36.51	18.70	24.11
Th	304.68	260.26	305.73	177.33	234.24	483.14	418.34	401.81	442.80	402.59
U	553.11	464.03	615.88	493.79	424.24	1635.17	892.47	1823.05	1029.74	850.72
	Granodiorite transition zone									
	VRU 29-1	VRU 29-4	VRU 29-6	VRU 29-8	VRU 29-12	VRU 40-1	VRU 40-5	VRU 40-10	VRU 40-11	VRU 40-13
P	606	653	317	208	415	1546	142	169	611	388
Ti	10.92	6.76	4.06	1.92	16.97	97.91	4.01	4.19	2.06	3.59
V	2.02	0.51	0.41	0.19	2.99	8.88	0.22	–	0.53	0.27
Mn	0.80	2.64	0.32	0.27	6.55	22.83	0.26	0.28	2.00	1.92
Rb	1.23	0.29	0.38	0.26	0.32	0.65	0.15	0.13	0.22	0.16
Sr	0.77	0.37	0.45	0.33	0.71	2.34	0.20	0.15	0.56	0.65
Y	5577	783	1184	955	1133	1215	647	496	923	670
Zr	372764	329433	396616	375106	404154	438356	413209	415989	373090	383530
Nb	22.83	7.03	7.58	8.14	10.25	7.23	3.57	2.45	5.17	4.48
La	0.34	10.16	0.31	0.10	0.82	4.14	0.05	0.02	0.71	1.01
Ce	147.51	47.30	24.97	25.05	35.64	45.77	15.97	13.75	23.62	27.08
Pr	2.79	3.84	0.16	0.04	0.24	1.50	0.03	0.04	0.41	0.27
Nd	37.49	9.87	1.28	0.57	1.52	8.01	0.48	0.49	2.41	1.73
Sm	59.60	2.97	3.40	2.07	2.25	4.89	1.07	1.31	2.91	1.80
Eu	22.38	0.64	0.74	0.54	0.78	1.55	0.54	0.33	0.79	0.56
Gd	220.86	11.80	18.74	12.79	16.74	20.58	6.84	6.09	14.99	10.25

Table 3 continued

	Granodiorite transition zone									
	VRU 29-1	VRU 29-4	VRU 29-6	VRU 29-8	VRU 29-12	VRU 40-1	VRU 40-5	VRU 40-10	VRU 40-11	VRU 40-13
Tb	58.31	4.33	7.55	5.43	6.68	7.35	2.68	2.13	5.34	3.63
Dy	631.79	59.75	96.92	72.27	81.71	97.98	37.46	29.56	71.30	46.76
Ho	201.17	23.59	37.74	29.90	37.12	37.03	15.25	12.78	31.68	18.82
Er	843.04	126.48	187.41	150.18	198.65	186.24	87.76	67.31	148.67	108.12
Tm	147.16	26.70	43.04	35.38	44.25	43.07	21.34	17.60	32.37	24.49
Yb	1419.5	330.1	450.1	378.1	459.0	491.1	291.7	246.4	349.9	284.4
Lu	248.26	52.23	86.46	78.59	101.73	99.52	56.11	39.49	71.46	58.12
Hf	7573	8956	10470	10157	10434	9349	8814	9285	9609	9573
Ta	6.33	3.36	4.46	4.91	5.09	3.72	1.52	1.31	3.02	2.23
Pb	91.81	73.11	43.10	35.00	36.57	32.89	12.44	8.88	25.22	24.87
Th	3395.39	207.50	480.62	413.67	514.46	737.57	241.41	214.83	429.27	600.83
U	4595.77	1315.51	2104.88	1681.28	1651.08	1673.83	640.03	509.02	1219.71	1206.21

Values are given in ppm

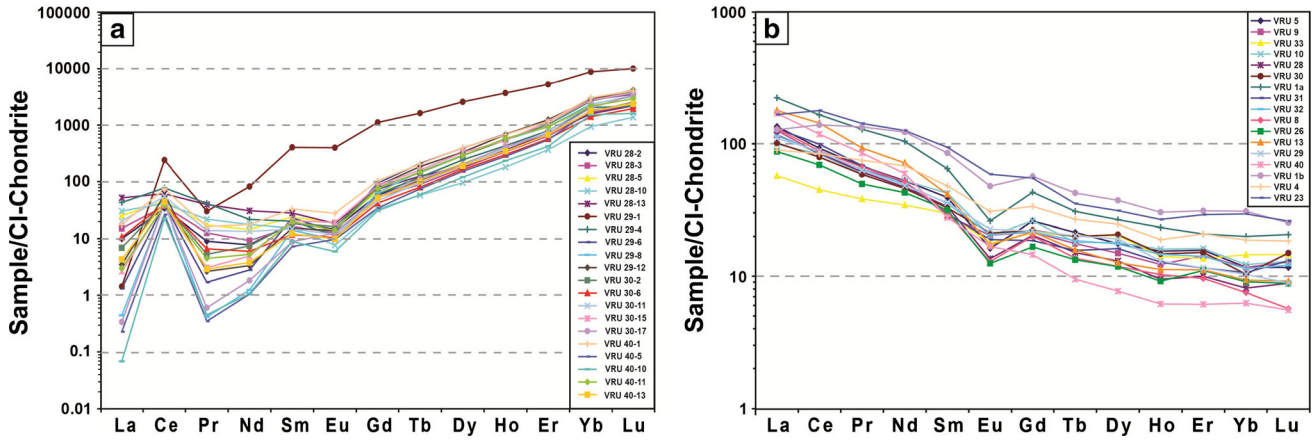

Fig. 9 **a** Rare earth elements patterns for zircons from granodiorites and tonalites of the transition zone. **b** Rare earth elements patterns for bulk rocks. Both diagrams are normalized to CI-chondrite (McDonough and Sun 1995)

of Ce^{3+}) in zircon (Hinton and Upton 1991; Thomas et al. 2002; Hoskin and Schaltegger 2003). Furthermore, zircons display a negative Eu anomaly ($Eu_N/Eu^* = 0.28–0.61$, and 0.49–0.84 for bulk rock; $Eu^* = (Sm_N \cdot Gd_N)^{1/2}$) indicative for plagioclase fractionation (that was also recognized in the trace element analyses for the bulk rock; Fig. 9b), and in contrast to the bulk rock trends, a steeply positive slope from medium REE to heavy REE ($(Lu/Gd)_N = 9.1–73.5$; 0.28–0.70 for bulk rock). All these features indicate that the zircons have an igneous origin (Hoskin and Schaltegger 2003). In magmatic zircons the higher compatibility of the HREE can be explained by the fact that they have smaller ionic radii in respect to the LREE and therefore substitute Zr^{4+} in the zircon crystals more effectively than the LREE (Hanchar and van Westrenen 2007).

Similar to trace elements in the bulk rocks (Fig. 9b), a trace element trend common to all zircons can be recognized (with the exception for VRU 29-1, which displays up to one order of magnitude higher values for some elements), indicating a single origin for the magma that generated the crystals.

7.4 TIMS dating of transition zone rocks

Results of the U–Pb dating are reported in Table 4. For reasons of clarity only concordant or sub-concordant analyses in, or approaching, the time span between 32 and 30 Ma were represented in the Wetherill diagrams (see Fig. 10a–d). Older concordant points were always considered as inherited from older crustal material, whereas very

Table 4 U–Pb ID-TIMS zircon isotope data for samples from the Bergell intrusion and the Como molasse

Sample[a]	Rock type	Wt. (mg)[b]	Compositional parameters							$^{208}Pb_g/^{206}Pb$
			U (ppm)[c]	Th^d/U	Pb (ppm)[c]	Pb^*/Pbc[e]	Pb* (pg)[e]	Pbc (pg)[e]	$^{206}Pb/^{204}Pb$[f]	
VRU28-1	Tonalite transition zone	0.015	1253	0.416	6.6	23.6	92.1	3.91	1497	0.133
VRU28-2	Tonalite transition zone	0.005	1088	0.438	9.1	1.4	28.6	19.87	108	0.141
VRU28-3	Tonalite transition zone	0.007	1793	0.336	19.1	18.6	132.2	7.12	1202	0.113
VRU28-7	Tonalite transition zone	0.007	883	0.426	4.8	10.8	28.8	2.66	697	0.137
VRU28-8	Tonalite transition zone	0.006	1215	0.304	6.4	9.9	34.6	3.51	656	0.098
VRU28-9	Tonalite transition zone	0.006	1692	0.184	7.9	17.8	46.6	2.61	1212	0.060
VRU28-10	Tonalite transition zone	0.024	497	0.415	2.6	19.4	60.0	3.09	1238	0.134
VRU28-11	Tonalite transition zone	0.006	2380	0.379	12.2	18.0	71.7	3.98	1160	0.122
VRU28-12	Tonalite transition zone	0.006	1228	0.450	6.4	18.7	37.1	1.99	1179	0.145
VRU30-1	Tonalite transition zone	0.012	1374	0.302	6.6	61.3	79.8	1.30	3975	0.097
VRU30-2	Tonalite transition zone	0.010	1774	0.301	8.6	62.3	83.0	1.33	4040	0.097
VRU30-3	Tonalite transition zone	0.011	1015	0.291	4.9	57.1	51.1	0.89	3709	0.094
VRU30-4	Tonalite transition zone	0.004	2135	0.2962	10.4	34.4	44.7	1.15	2289	0.095
VRU30-5	Tonalite transition zone	0.005	1372	0.371	7.0	20.3	30.1	1.49	1302	0.119
VRU30-6	Tonalite transition zone	0.004	1073	0.285	5.7	8.8	20.8	2.37	589	0.092
VRU29-1	Granodiorite transition zone	0.008	1132	0.255	36.3	121.3	294.9	2.43	7922	0.083
VRU29-2	Granodiorite transition zone	0.007	1978	0.317	9.8	34.7	61.8	1.78	2252	0.102
VRU29-3	Granodiorite transition zone	0.012	1742	0.266	8.6	17.9	93.6	5.23	1189	0.086
VRU29-4	Granodiorite transition zone	0.010	1830	0.364	22.7	0.7	91.3	133.8	62.1	0.117
VRU29-5	Granodiorite transition zone	0.004	878	0.284	4.4	14.3	17.6	1.23	945	0.091
VRU29-6	Granodiorite transition zone	0.010	2072	0.305	9.0	15.4	87.0	5.64	1016	0.098
VRU29-8	Granodiorite transition zone	0.007	1561	0.298	7.6	35.2	50.8	1.4	2293	0.096

Sample[a]	Rock type	Radiogenic isotope ratios							$^{207}Pb_i/^{206}Pb$	Isotopic ages				
		$^{207}Pb_g/^{206}Pb$	% err[h]	$^{207}Pb_g/^{235}U$	% err[h]	$^{206}Pb_g/^{238}U$	% err[h]	Corr. coef.		±[h]	$^{207}Pb_i/^{235}U$	±[h]	$^{206}Pb_i/^{238}U$[i]	±[h]
VRU28-1	Tonalite transition zone	0.046546	0.208	0.031942	0.260	0.004977	0.109	0.636	26.00	4.98	31.93	0.08	32.00	0.03
VRU28-2	Tonalite transition zone	0.046500	1.151	0.031189	1.177	0.004865	0.338	0.220	23.65	27.58	31.18	0.36	31.28	0.11
VRU28-3	Tonalite transition zone	0.049867	0.128	0.069480	0.185	0.010105	0.075	0.853	188.82	2.97	68.21	0.12	64.81	0.05
VRU28-7	Tonalite transition zone	0.046687	0.413	0.031335	0.453	0.004868	0.117	0.461	33.25	9.88	31.33	0.14	31.30	0.04
VRU28-8	Tonalite transition zone	0.046698	0.323	0.031130	0.365	0.004835	0.091	0.561	33.82	7.72	31.13	0.11	31.09	0.03
VRU28-9	Tonalite transition zone	0.046891	0.250	0.030306	0.345	0.004688	0.206	0.695	43.68	5.97	30.32	0.10	30.15	0.06
VRU28-10	Tonalite transition zone	0.046675	0.190	0.031443	0.198	0.004886	0.059	0.294	32.61	4.54	31.43	0.06	31.42	0.02
VRU28-11	Tonalite transition zone	0.046689	0.211	0.031230	0.257	0.004851	0.091	0.632	33.33	5.05	31.23	0.08	31.20	0.03
VRU28-12	Tonalite transition zone	0.046670	0.277	0.031239	0.316	0.004855	0.080	0.579	32.39	6.64	31.23	0.10	31.22	0.02
VRU30-1	Tonalite transition zone	0.046634	0.028	0.031224	0.067	0.004856	0.061	0.909	30.52	0.67	31.22	0.02	31.23	0.02
VRU30-2	Tonalite transition zone	0.046627	0.134	0.031322	0.178	0.004872	0.123	0.657	30.16	3.22	31.32	0.05	31.33	0.04
VRU30-3	Tonalite transition zone	0.046622	0.098	0.031203	0.247	0.004854	0.204	0.922	29.90	2.35	31.20	0.08	31.22	0.06
VRU30-4	Tonalite transition zone	0.046643	0.129	0.031252	0.208	0.004860	0.123	0.815	30.97	3.10	31.25	0.06	31.25	0.04
VRU30-5	Tonalite transition zone	0.046641	0.199	0.031357	0.261	0.004876	0.112	0.706	30.90	4.76	31.35	0.08	31.36	0.03
VRU30-6	Tonalite transition zone	0.046625	0.277	0.031179	0.333	0.004850	0.103	0.659	30.08	6.62	31.17	0.10	31.19	0.03
VRU29-1	Granodiorite transition zone	0.051827	0.072	0.232652	0.219	0.032558	0.187	0.950	277.78	1.65	212.39	0.42	206.5	0.38
VRU29-2	Granodiorite transition zone	0.046643	0.111	0.031375	0.226	0.004879	0.167	0.884	30.98	2.65	31.37	0.07	31.37	0.05
VRU29-3	Granodiorite transition zone	0.046641	0.152	0.030949	0.227	0.004813	0.122	0.783	30.89	3.64	30.95	0.07	30.95	0.04
VRU29-4	Granodiorite transition zone	0.046655	3.289	0.032469	3.381	0.005047	0.713	0.232	31.58	78.71	32.44	1.08	32.46	0.23
VRU29-5	Granodiorite transition zone	0.046620	0.281	0.030646	0.340	0.004768	0.118	0.630	29.80	6.73	30.65	0.10	30.66	0.04
VRU29-6	Granodiorite transition zone	0.046574	0.156	0.026673	0.215	0.004154	0.088	0.785	27.43	3.74	26.73	0.06	26.72	0.02
VRU29-8	Granodiorite transition zone	0.046698	0.185	0.031004	0.225	0.004815	0.087	0.610	33.79	4.43	31.00	0.07	30.97	0.03

Table 4 continued

Sample[a]	Rock type	Wt. (mg)[b]	Compositional parameters							$^{208}Pb_g/^{206}Pb$
			U (ppm)[c]	Th^d/U	Pb (ppm)[c]	Pb^*/Pb_c[e]	Pb* (pg)[e]	Pbc (pg)[e]	$^{206}Pb_f/^{204}Pb$	
VRU40-1b	Granodiorite transition zone	0.018	2964	0.304	14.4	48.9	247.3	5.1	3187	0.098
VRU40-1	Granodiorite transition zone	0.032	2122	0.302	10.3	46.0	327.5	7.1	2998	0.097
VRU40-2	Granodiorite transition zone	0.018	1507	0.310	7.3	60.3	129.0	2.1	3905	0.100
VRU40-2b	Granodiorite transition zone	0.018	1507	0.318	7.4	103.4	132.2	1.3	6655	0.102
VRU40-3	Granodiorite transition zone	0.006	734	0.465	24.5	9.0	123.6	13.8	565	0.163
VRU40-4	Granodiorite transition zone	0.016	44	0.238	0.3	1.5	3.1	2.1	116	0.081
VRU40-5	Granodiorite transition zone	0.011	3226	0.334	16.8	13.0	167.0	12.9	853	0.107
VRU40-6	Granodiorite transition zone	0.007	1257	0.339	22.9	0.4	44.0	107	45	0.119
VRU40-7	Granodiorite transition zone	0.010	1897	0.344	9.4	33.3	94.0	2.8	2146	0.111
VRU40-8	Granodiorite transition zone	0.009	2145	0.278	10.3	43.2	92.4	2.1	2830	0.090
CMB4-1	Tonalite Como molasse	0.013	221	0.575	1.3	8	12.4	1.84	517	0.185
CMB4-2	Tonalite Como molasse	0.006	214	0.513	1.4	4	5.5	1.63	268	0.165
CMB4-3	Tonalite Como molasse	0.013	224	0.485	1.3	8	12.7	2.02	483	0.156
CMB4-6	Tonalite Como molasse	0.008	461	0.332	2.5	9	15.9	1.94	624	0.107
CMB4-7	Tonalite Como molasse	0.013	287	0.298	1.6	8	16.0	2.22	552	0.096
CMB4-4	Tonalite Como molasse	0.009	482	0.288	2.5	13	17.9	1.57	859	0.093
CMB4-5	Tonalite Como molasse	0.007	368	0.314	2.1	7	10.7	1.82	451	0.101

Sample[a]	Rock type	Radiogenic isotope ratios							$^{207}Pb_i/^{206}Pb$	Isotopic ages				
		$^{207}Pb_g/^{206}Pb$	% err[h]	$^{207}Pb_g/^{235}U$	% err[h]	$^{206}Pb_g/^{238}U$	% err[h]	Corr. coef.		±[h]	$^{207}Pb_i/^{235}U$	±[h]	$^{206}Pb_i/^{238}U$	±[h]
VRU40-1b	Granodiorite transition zone	0.046736	0.225	0.031283	0.440	0.004855	0.383	0.858	35.75	5.39	31.28	0.14	31.22	0.12
VRU40-1	Granodiorite transition zone	0.046684	0.233	0.031237	0.443	0.004853	0.383	0.851	33.07	5.58	31.23	0.14	31.21	0.12
VRU40-2	Granodiorite transition zone	0.046599	0.148	0.031062	0.240	0.004834	0.158	0.799	28.72	3.54	31.06	0.07	31.09	0.05
VRU40-2b	Granodiorite transition zone	0.046646	0.085	0.031789	0.238	0.004943	0.204	0.938	31.15	2.03	31.78	0.07	31.78	0.06
VRU40-3	Granodiorite transition zone	0.055348	0.190	0.218956	0.246	0.028691	0.102	0.692	426.32	4.24	201.04	0.45	182.35	0.18
VRU40-4	Granodiorite transition zone	0.049221	1.890	0.031258	2.011	0.004606	0.222	0.583	158.35	44.18	31.25	0.62	29.62	0.07
VRU40-5	Granodiorite transition zone	0.046711	0.171	0.031467	0.265	0.004886	0.162	0.782	34.48	4.10	31.46	0.08	31.42	0.05
VRU40-6	Granodiorite transition zone	0.050988	3.393	0.037137	3.303	0.005283	1.151	0.095	240.28	78.14	37.03	1.20	33.96	0.39
VRU40-7	Granodiorite transition zone	0.046822	0.195	0.031265	0.249	0.004843	0.126	0.638	40.13	4.65	31.26	0.08	31.14	0.04
VRU40-8	Granodiorite transition zone	0.046816	0.150	0.030984	0.203	0.004800	0.101	0.706	39.85	3.59	30.98	0.06	30.87	0.03
CMB4-1	Tonalite Como molasse	0.046671	0.588	0.032145	0.614	0.004995	0.076	0.391	32.45	14.07	32.13	0.19	32.12	0.02
CMB4-2	Tonalite Como molasse	0.046672	1.462	0.032133	1.525	0.004993	0.180	0.399	32.46	34.98	32.11	0.48	32.11	0.06
CMB4-3	Tonalite Como molasse	0.046665	0.655	0.032115	0.679	0.004991	0.104	0.309	32.12	15.67	32.10	0.21	32.10	0.03
CMB4-6	Tonalite Como molasse	0.046665	0.488	0.032019	0.508	0.004976	0.081	0.324	32.14	11.67	32.00	0.16	32.00	0.03
CMB4-7	Tonalite Como molasse	0.046669	0.472	0.032027	0.492	0.004977	0.080	0.334	32.33	11.29	32.01	0.16	32.01	0.03
CMB4-4	Tonalite Como molasse	0.046664	0.502	0.031985	0.518	0.004971	0.088	0.254	32.04	12.02	31.97	0.16	31.97	0.03
CMB4-5	Tonalite Como molasse	0.046663	0.719	0.032011	0.749	0.004975	0.099	0.363	32.02	17.19	31.99	0.24	31.99	0.03

[a] Labels for fractions composed of single zircon grains or fragments; all zircons are annealed-leached (after Mattinson 2005)

[b] Nominal fraction weights measured after chemical abrasion

[c] Nominal U and total Pb concentrations subject to uncertainty in weighting zircons

[d] Model Th/U ratio calculated from radiogenic $^{208}Pb/^{206}Pb$ ratio, assuming concordance

[e] Pb* and Pbc represent radiogenic and common Pb, respectively

[f] Measured ratio corrected for spike and fractionation only

[g] Corrected for fractionation, spike, and common Pb; the composition of the procedure blank: $^{206}Pb/^{204}Pb = 18.08 \pm 0.22$ %; $^{207}Pb/^{204}Pb = 15.62 \pm 0.28$ %; $^{208}Pb/^{204}Pb = 38.0\ 5 \pm 0.59$ %, the procedure blank was estimated between 0.5–1.5 ppb; the common Pb correction according Stacey and Kramers (1975) at 31 Ma (all uncertainties 2-sigma). $^{206}Pb/^{238}U$ and $^{207}Pb/^{206}Pb$ ratios corrected for initial disequilibrium in $^{230}Th/^{238}U$

[h] Errors are 2-sigma, propagated using the algorithms of Schmitz and Schoene (2007) and Crowley et al. (2007)

[i] Calculations are based on the decay constants of Jaffey et al. (1971). $^{206}Pb/^{238}U$ and $^{207}Pb/^{206}Pb$ ages corrected for initial disequilibrium in $^{230}Th/^{238}U$

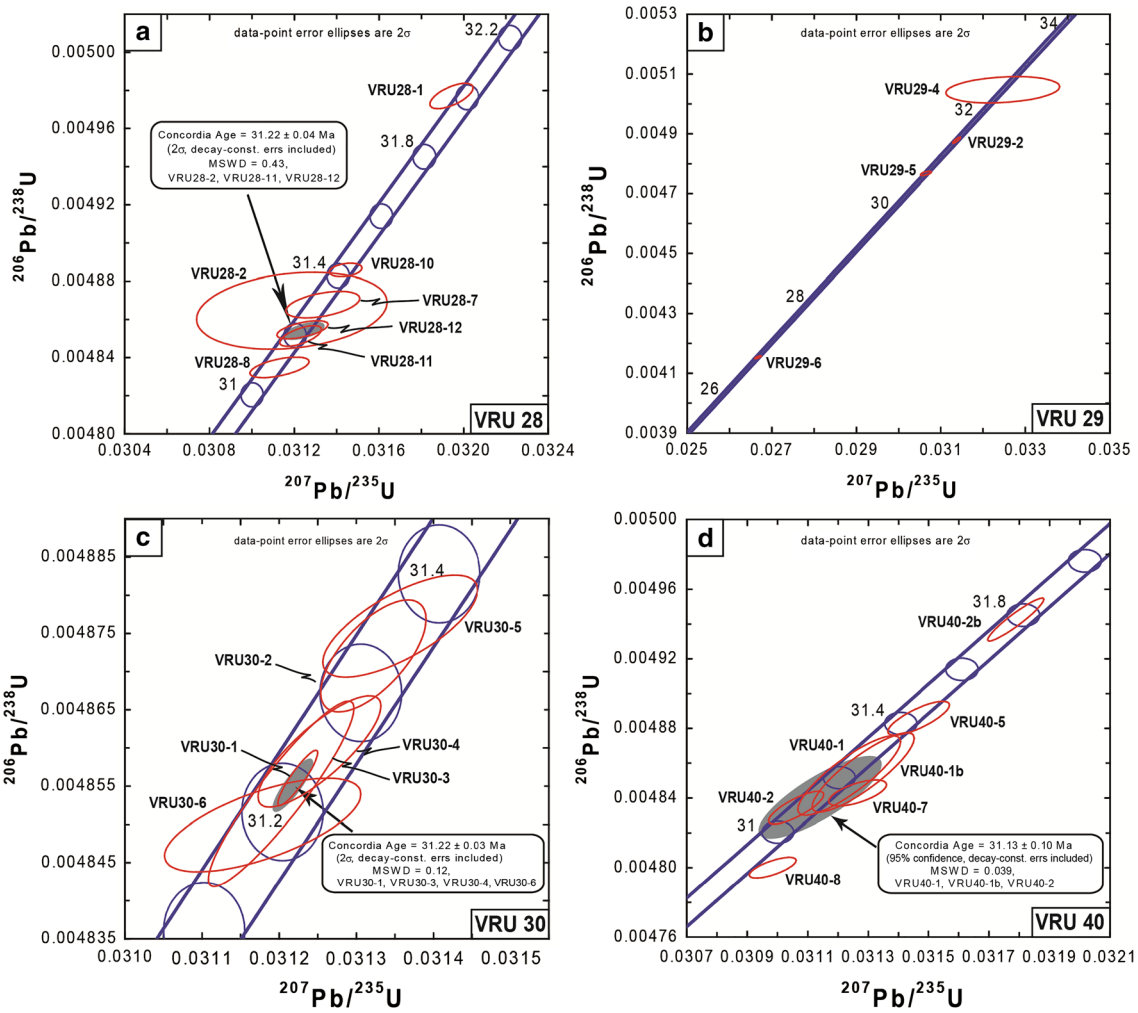

Fig. 10 Concordia diagrams for zircons dated in the transition zone. **a–c** K-feldspar rich tonalites. **b–d** Granodiorites

young ages were interpreted as resulting from Pb loss. In VRU 28 most of the analyzed zircons plot on the Concordia curve between 31.0 and 31.4 Ma, but one zircon plots outside this range at 32 Ma, which is however consistent with the previous age determinations of von Blanckenburg (1992) for the tonalite of the easternmost part of the pluton. A Concordia age (Ludwig 2000) calculated for the overlapping zircon analyses gave 31.22 ± 0.04 Ma (MSWD = 0.43). On the other hand, in VRU 30 all the measured zircons lie between 31.2 and 31.4 Ma, with a Concordia age determined at 31.22 ± 0.03 Ma (MSWD = 0.12).

For what concerns the analysis of granodiorite samples, VRU 29 displays a clear scattering along the Concordia curve, with values ranging from 26.72 Ma (VRU29-6) to 32.46 Ma (VRU29-4), and a major drawback that it was not possible to calculate a Concordia age. Zircons of VRU 40 instead show a more clustered behavior between 31.0 and 31.4 Ma also if one zircon plots at 31.8 Ma. The related Concordia age is 31.13 ± 0.10 Ma (MSWD = 0.039).

For a comparison, analyses of zircons from the transition zone were plotted in a Concordia diagram together with other U–Pb measurements of zircons, titanites and allanites available in the literature (Fig. 11). We also report the 31.5 ± 0.2 Ma age range for a cumulate cpx-amphibole-gabbro enclosed in tonalite, obtained by von Blanckenburg (1989). This age is slightly younger than the host tonalite (31.9 ± 0.1 Ma).

In general, the analyzed zircons from the transition zone display smaller error ellipses than data reported in the literature. This can be ascribed to the different method adopted during this study for the preparation of the zircons before dissolution. Moreover, the discrete age range, which is always assumed for tonalite and granodiorite (i.e. 32 Ma for tonalite and 30 Ma for granodiorite) is not observable for the zircons from the transition zone, because the

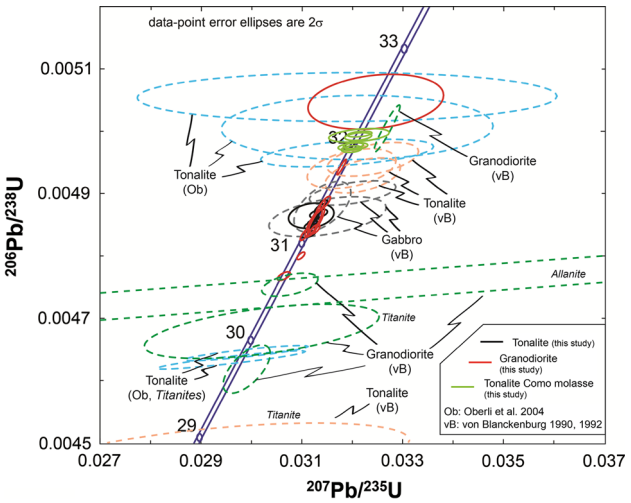

Fig. 11 Concordia diagram for the measured zircons of the transition zone (*black* for tonalite, *red* for granodiorite) and of the tonalite sample CMB-4 sedimented into the Como molasse (*solid green line*) compared to U–Pb radiometric analyses of different minerals (zircons, titanites and allanite) from the literature (*dashed ellipses*). If not specified in the figures, the ellipses refer to zircon analyses. Literature data are from von Blanckenburg (1989, 1992) and Oberli et al. (2004)

majority of the analyses cluster around 31.2 Ma. It is interesting to notice that this age is similar to the age obtained for the cumulate gabbro (von Blanckenburg 1989).

7.5 TIMS dating of Bergell boulders from the Como molasse

Seven zircon grains from one representative tonalite of the Como molasse were dated. The zircons form two distinct groups. The first set (CMB4-4, CMB4-5, CMB4-6 and CMB4-7) plots at ~32.0 Ma (with a calculated Concordia age of 31.99 ± 0.04 Ma, MSWD = 0.0005), whereas the second group of zircons (CMB4-1, CMB4-2 and CMB4-3) plots at ~32.1 Ma (with a calculated Concordia age of 32.12 ± 0.04 Ma, MSWD = 0.0023). This confirms that the tonalites of the Como molasse are not only mineralogically (and geochemically as discussed below) but also in their intrusion age part of the main tonalite unit of the Bergell.

8 Discussion

8.1 Bulk rock chemistry of the Bergell intrusives

In order to place the transition zone and the boulders of the Como molasse in the context of the entire Bergell batholith, we have compiled all available bulk rock analyses (see electronic appendix, data sources from Weibel 1960; Moticska 1970; Wenk et al. 1977; Reusser 1980; Morand 1981; Reusser 1987; Diethelm 1989; von Blanckenburg et al. 1992; Oberli et al. 2004; Vogel 2010) as well as for the peraluminous intrusion of the Novate granite (Moticska 1970; Wenk et al. 1977; Reusser 1980; Morand 1981; Reusser 1987; Hafner 1993). Secondly, to compare the Bergell with other calc-alkaline batholiths, we employed compilations of the Peninsular Range batholith (Lee et al. 2007) and of the south Alpine 42–29 Ma old (Del Moro et al. 1983) Adamello batholith (compiled by P. Ulmer, pers.comm.).

The compilation of the complete set of Bergell bulk rock analyses reveals that both the main granodiorite as well the main tonalite units display a wide range of SiO_2-concentrations (from 53 to 68 wt% for the main tonalite and from 60 to 75 wt% for the main granodiorite unit) which co-vary negatively with CaO, FeO, MgO, MnO and TiO_2 (Fig. 5). For each of these major elements the main tonalite and granodiorite units have a wide and overlapping range defining a continuous fractionation trend from a gabbroic to a granitic composition. Remarkably, X_{Mg} varies only from 0.6 to 0.4 over a range from 43 to 75 wt% SiO_2. On the low-Si end, only the cumulative hbl-gabbros and hornblendites have higher X_{Mg} values while on the high Si-end only the granitic dykes decrease to an X_{Mg} of 0.05. The major elements of the tonalites and granodiorites of the transition zone unit (and also those of the Como molasse) are completely congruent with the trend defined by the main tonalite and granodiorite units. The Bergell intrusion is hence composed of three chemically heterogeneous main units which compositional ranges results mainly from a variation of mineral mode rather than of the mineral assemblage present. This feature was already recognized on a petrographic level (e.g. Weibel 1960; Reusser 1987). The spatially unsystematic heterogeneity within these three units provides further strong support that these units did not represent single diapirs, but instead rose as multiple magma batches which together constitute a single amphibole-dominated liquid line of descent (Nandedkar et al. 2014). Contamination of the mantle source by crustal material and crustal assimilation accompanying the fractionation process was documented for the Bergell intrusion with Nd-isotopes by Blankenburg (1992) and Gregory et al. (2009).

Since most of the available analyses are XRF only, the concentrations of only few trace elements are measured for a majority of the samples. Co and Sc concentrations follow a typical depletion trend with increasing SiO_2 mirroring the depletion in e.g. FeO. Zr-patterns are more complicated: for the tonalite and granodiorite main units, Zr concentrations increase with SiO_2 while for the transition zone unit Zr decreases with SiO_2, pointing to early zircon saturation in the parental magma of this latter unit (Fig. 6f). The high

Zr-concentrations mainly in the transition zone granodiorites could be explained by zirconium accumulation or by a parental melt similar to the suite of calc-alkaline basic dykes and xenoliths (Diethelm 1989). This peculiarity is also supported by the distribution of trace elements normalized to N-MORB or chondrite, which for the transition zone show a cogenetic origin for the mafic inclusions and intermediate members. Similar to Zr, P is much higher in the transition zone tonalites than in the rocks of the main tonalite unit (Fig. 5j). These features support the finding from age dating, that the transition zone cannot result from simple mixing of the tonalite and granodiorite main units but represents an individual melt batch or unit which parent magma had higher Zr and P concentrations than that of the tonalite or granodiorite main units.

Variations in Ba, Sr, Rb, and also K_2O and Na_2O within the Bergell intrusives are more complex as their behavior is governed by the fractionation and accumulation of mainly feldspars. Ba reaches maximum concentrations in the granodiorite of the transition zone and main units which can be explained by the strong partitioning of this element into the K-feldspar megacrysts. Moreover, the differences in Ba, Rb and Sr concentrations of some aplites and pegmatites crosscutting the Bergell intrusives on one side and the Novate granite on the other side indicate that these granite dykes do not belong to the same magmatic series.

Relatively complete trace element analyses of Bergell intrusives are scarce (Fig. 7a, b, Mottana et al. 1978; Diethelm 1989; von Blanckenburg 1989) but allow for the following observations: (1) the tonalites of the transition zone display a slight enrichment compared to the main tonalite, except for Ti and heavy REE (HREE), (2) the granodiorite of the transition zone follows the same trend as the main granodiorite unit except for a slight enrichment in Ti and HREE, (3) the basic dykes and xenoliths show a wide normalized concentration spectrum, which partly overlap the trends for the intermediate rocks both of the main and transition zone units, (4) similarly, the early differentiates (mainly hornblendites, hbl-gabbro and gabbro) also display a wide concentration spectrum with a tendency of depletion compared to the intermediate rocks (except for Ti and heavy REE). All of these similarities suggest similar fractionation series for the three main units, i.e. the tonalite, transition zone and granodiorite. Nevertheless, the observed slight but distinct differences argue in favor of different episodes with slightly different parental melts rising from the mantle into the crust over several million years.

The Novate granite and some of the acidic dykes (aplites, pegmatites and one leucogranitic stock) are depleted compared to the transition zone and the main tonalite and granodiorite units (Fig. 7a–c), demonstrating that a number of acidic dykes crossing the Bergell intrusion do not result from fractionation within the calc-alkaline batholith. This is in line with the younger age of the Novate granite (24.0 ± 1.2 Ma) and an isotopic geochemistry characteristic for S-type granites (von Blankenburg et al. 1992; Liati et al. 2000).

8.2 Comparison to other calc-alkaline batholiths

Little difference appears when comparing the major and trace element compositions (see Figs. 5a–j, 6a–f, 7a–d) of the Bergell suite with the Adamello batholith and the Peninsular Range Batholith (southern California). The only significant difference for the main trend is a slight enrichment of K_2O-concentrations in the Bergell, which is mirrored by Rb-concentrations. In contrast to the Adamello and Peninsular range batholiths, shoshonitic dykes are abundant in the Bergell.

The lack of large differences between the Bergell and the two reference calc-alkaline batholiths chosen here is remarkable. The compiled bulk rock analyses of the Bergell characterize this intrusive suite as typical calc-alkaline, with a complete range of SiO_2-concentrations (ranging from about 43 to 75 wt%) along an amphibole dominated liquid line of descent (Nandedkar et al. 2014). Calc-alkaline trends are only found in subduction-related arc magmatism, but in the Alps it has to be stressed that the two major magmatic bodies (Bergell and Adamello) occur on both sides of the Periadriatic Fault that marks the plate boundary between the (northern) subducting plate and the southern overriding plate. The Bergell intrusion constitutes in fact a batholith that intruded into the subducting plate rather than the overriding plate. Davies and von Blanckenburg (1995) and von Blanckenburg and Davies (1995) explained this behavior as a result of a thermal anomaly at the base of the colliding continental lithosphere(s) induced by the break off of the European slab. The break off allowed the asthenospheric mantle to rise and to melt the sub-Adriatic subduction-enriched lithospheric mantle (von Blanckenburg et al. 1992). In this model, in a later stage of steepening of the suture and back-thrusting, the molten material was emplaced in the overriding African plate as well in the formerly down-going European plate. The lack of substantial differences in geochemistry between the Bergell and the Adamello batholiths corroborates this hypothesis.

8.3 Zircon U/Pb ages and the timing of the Bergell intrusion

Our high precision U–Pb zircon ages allow us to determine a range of crystallization ages for the transition zone unit of the Bergell pluton and consequently to constrain its evolution. Our results fall in between the intrusion ages

determined by von Blanckenburg (1992) for the tonalite (31.88 ± 0.09 Ma) and granodiorite units (30.13 ± 0.17 Ma), where the tonalite age is a concordant U/Pb zircon age while for the granodiorite is a U/Pb age of sphene. In von Blanckenburg (1992) three granodiorite zircons yielded concordant ages of 29.0–30.7 Ma and one grain that was very rich in common lead gave 26.3 Ma and was dismissed. The crystallization of the transition zone tonalites and granodiorites occurred over a time span ranging from at most 31.26 Ma (tonalite) to 31.03 Ma (granodiorite), i.e. a relatively short time, which including all errors does not span more than ~0.5 Ma. In this period tonalitic and granodioritic magma phenotypes coexisted, then, the Bergell magmatism turned from tonalitic to granodioritic in composition. The 31.2 Ma also characterizes the beginning of the large scale zoning as observable today in the Bergell pluton.

The contemporaneous crystallization of the transition zone granodiorites and tonalites is in agreement with the lack of unambiguous relative intrusives relationships between these two rock types in the transition zone outcropping in Valle dei Ratti. For what concerns the other granodiorite sample (VRU 29), and also for the main unit granodiorite of von Blanckenburg (1992), individual zircons are scattered along the Concordia curve. Von Blanckenburg (1992) explained this pattern by invoking a possible Pb loss due to high U concentrations, which may cause radiation damage in the zircon crystals. This argumentation cannot be applied to zircons of sample VRU 29 because they do not have significantly higher U concentrations than those of other samples. For the zircon sample VRU 29-4 reworking or inheritance from the main tonalitic unit would explain the age of 32.46 ± 0.23 Ma. The youngest age for the grain VRU 29-6 is more difficult to interpret, similar to the one grain sample of von Blanckenburg (1992), it falls outside the time interval of the protracted crystallization history of the Bergell pluton. This history ranges from 33 to 28 Ma, as determined using zircons and sphene of a tonalite sample collected in the westward tonalite tail (Oberli et al. 2004). Therefore we suggest that the young age for VRU 29-6 may reflect post-crystallization loss of Pb along micro-cracks by fluid interactions (Geisler et al. 2007) or re-melting due to local fluid infiltration during the protracted Barrovian metamorphism of this region (Rubatto et al. 2009).

8.4 Formation mechanism of the "transition zone" unit

The historical perception of the Bergell transition zone as a mixing zone between the main tonalite and granodiorite units cannot be maintained. Instead, the transition zone is both, in time and trace element geochemistry, a unit well distinct from the other two main units. In particular the transition zone intrusives are older than the granodiorite unit, excluding any mixing in a deep seated magma reservoir. Also, the presently known few high precision ages stretch from ~33 to ~28 Ma, i.e. over 5 million years, which is far beyond the life time of any single magma pulse. We thus conclude that the Bergell was formed during at least three main intrusive pulses which all yielded a suite of evolved rocks, with SiO_2-ranges of 53–68 wt% for the main tonalite, 54–71 wt% for the transition zone unit (excluding the mingled mafic enclaves and the late crystallized aplitic and pegmatitic dykes) and 60–75 wt% for the main granodiorite unit. The transition zone itself is made up by a series of intrusive stocks which are strongly deformed in upper Valle dei Ratti and now form a series of bands typically 5–20 m wide that can be followed over up to hundreds of meters. At the NW rim of the Bergell (Val Codera), where less deformation is present, these stocks are clearly discordant and several tens of meters large.

The main deformation of the central Bergell intrusives was ascribed to synmagmatic emplacement and folding, which is more intense in the southern part (Davidson et al. 1996). These authors describe the Bergell as a more nappe like structure forming in a late intrusive stage where the pluton is still partially molten. The textural observation in the banded part of the transition zone is in full agreement with such an interpretation.

8.5 Significance of the Bergell intrusives in the Como molasse

The geochemical characterization and age dating of the tonalite and granodiorite boulders in the Como molasse south of Chiasso confirm them as Bergell intrusives. Geobarometry reveals that these boulders originated from shallower intrusion levels than exposed today: the tonalites devoid of magmatic epidote yield intrusion pressures of 3.6 kbar while the present day exposed tonalites have intrusion pressures of 5.8 kbar and more. This leads to the following scenario: 32.0 ± 0.1 Ma the main tonalite unit intruded to a depth as shallow as 13.2 ± 2.9 km (3.6 ± 0.8 kbar) and 25 ± 1 Ma these tonalites were eroded and sedimented in the Como molasse south of the Bergell intrusion. To calculate the pressure and depth difference for the Como molasse boulders and the presently exposed intrusives, only precision (mostly resulting from mineral heterogeneity) but not the accuracy (of ±0.6 kbar for the Al-in-hbl barometer; Schmidt 1992) is required. In our samples precision is about 0.2 kbar for the average intrusion pressure of the main tonalite unit (normalized for an elevation of 1,582 m, representing the average altitude of all the samples analyzed for geobarometry) we obtain 6.5 ± 0.4 kbar (Reusser 1987; Davidson et al. 1996),

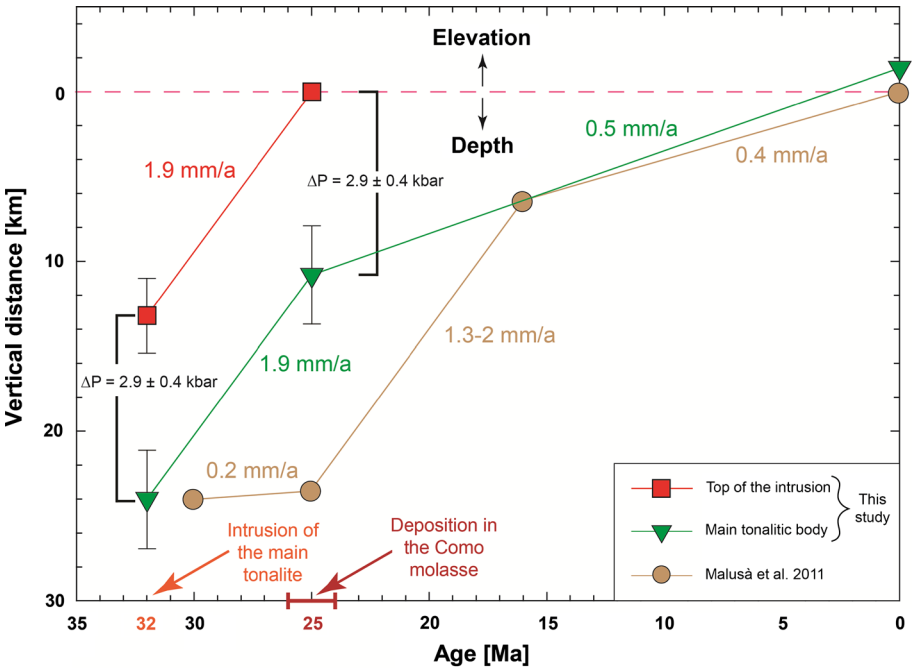

Fig. 12 Calculated average erosion rates for the Bergell intrusion. Error for the deposition age of the Como molasse is assumed to be at least 1 Ma, whereas the error for the intrusion age of the Bergell pluton is smaller than the symbols and therefore omitted

which consequently leads to an average intrusion depth difference of 10.7 ± 1.6 km (2.9 ± 0.4 kbar). Considering that the present lowest point of the main tonalite is at 200 m a.s.l (Novate Mezzola) the difference from the average altitude is approximately 1.4 km, to be added to the average intrusion depth. Hence, over the last 25 Myr at least 12.1 ± 1.6 km have been eroded. This results in average erosion rates of 1.9 ± 0.4 mm/a for the period 32–25 Ma and of 0.5 ± 0.1 mm/a in the last 25 Myr. The first value is in conflict with Malusà et al. (2011), who inferred an erosion rate of 0.2 mm/a between 30 and 25 Ma, then 1.3–1.4 mm/a (up to 2 mm/a for the western tail of the Bergell intrusion) from 25 to 16 Ma and finally 0.4 mm/a (for both tail and main body) from 16 Ma to present (see Fig. 12). Nevertheless our initial high erosion rate is consistent with the high exhumation rate of 2 mm/a recently calculated by Fox et al. (2014) and the high cooling temperature rates proposed for the Bergell intrusion (e.g. Wagner et al. 1977, 1979; Giger and Hurford 1989; Villa and von Blanckenburg 1991) as well as for the penninic units of the Lepontine dome (see e.g. Wagner et al. 1977; Vance and O'Nions 1992).

9 Conclusion

The Bergell intrusive displays a typical subduction-related calc-alkaline trend with the main fractionation series ranging from 43–75 wt% SiO_2. Even if the Bergell pluton sits in the initially subducting plate, there is no obvious chemical difference to calc-alkaline plutons such as the Adamello or the Peninsular Range Batholith, both located in the overriding plate. This supports a model where a subduction-modified mantle wedge is sucked into a region below the plate interface when the subducted slab breaks off (von Blanckenburg and Davies 1995).

The heterogeneity of each of the three mappable main units (granodiorite, tonalite and transition zone) suggests that the Bergell magmatism was characterized by multiple injections of melts that generally evolved with time. This heterogeneity is much more obvious in the variability of magmatic phenotypes in the transition zone unit, but equally present in the geochemistry of the main tonalite and granodiorite units. The transition zone unit consists of small stocks of well distinct intrusives characterized by magmatic flow structures such as compositional banding, schlieren, preferred orientation and accumulation of K-feldspar megacrysts and by magma mingling of mafic enclaves. Identical trace element signatures between the intermediate magmas and the mafic enclaves indicate a common magma source.

The available high precision U–Pb ages of zircons indicate that the Bergell pluton was built in (at least) three main phases, peaking at ~32.0 Ma for the tonalite unit, ~31.2 Ma for the transition zone unit and 30.2 for the granodiorite unit. Overall, 5 million years of calc-alkaline magmatic activity are documented, requiring several magmatic pulses originating from the mantle.

Acknowledgments We would like to thank L. Zehnder for the measurement of XRF glass pills, B. Brahimi and M. Wälle for the help with LA-ICP-MS and P. Ulmer for making available analyses of the Adamello batholith. We thank A. Berger and O. Reubi for their detailed comments. E. Gnos is also thanked for his helpful suggestions and the editorial handling of this manuscript.

References

Bateman, P. C., & Chappell, B. W. (1979). Crystallization, fractionation, and solidification of the Tuolumne Intrusive Series, Yosemite National Park, California. *Geological Society of America Bulletin, 90*, 465–482.

Berger, A. (1996). Geological-tectonic map of the Bergell pluton (1:50,000). *Schweizerische Mineralogische und Petrographische Mitteilungen*, *76*(Supplement)

Berger, A., & Gieré, R. (1995). Structural observations at the eastern contact of the Bergell Pluton. *Schweizerische Mineralogische und Petrographische Mitteilungen, 75*, 241–258.

Berger, A., Rosenberg, C., & Schmid, S. M. (1996). Ascent, emplacement and exhumation of the Bergell pluton within the Southern Steep Belt of the Central Alps. *Schweizerische Mineralogische und Petrographische Mitteilungen, 76*, 357–382.

Berger, A., & Stünitz, H. (1996). Deformation mechanisms and reaction of hornblende: examples from the Bergell tonalite (Central Alps). *Tectonophysics, 257*, 149–174.

Berger, A., Thomsen, T. B., Ovtcharova, M., Kapferer, N., & Mercolli, I. (2012). Dating emplacement and evolution of the orogenic magmatism in the internal Western Alps: 1. The Miagliano Pluton. *Swiss Journal of Geosciences, 105*, 49–65.

Bernoulli, D., Giger, M., & Müller, D. W. (1993). Sr-isotope-stratigraphy of the Gonfolite Lombarda Group ("South-Alpine Molasse", northern Italy) and radiometric constraints for its age deposition. *Eclogae Geologicae Helvetiae, 86*, 751–767.

Best, M. G. (2003). *Igneous and metamorphic petrology* (2nd ed., p. 752). Malden: Wiley-Blackwell Publishing.

Burri, T., Berger, A., & Engi, M. (2005). Tertiary migmatites in the Central Alps: regional distribution, field relations, conditions of formation, and tectonic implications. *Schweizerische Mineralogische und Petrographische Mitteilungen, 85*, 215–232.

Cornelius, H. P. (1915). Geologische Beobachtungen im Gebiet des Forno-Gletschers (Engadin). *Centralblatt für Mineralogie Geologie und Paläontologie, 8*, 246–252.

Crowley, J. L., Schoene, B., & Bowring, S. A. (2007). U–Pb dating in the Bishop Tuff at the millennial scale. *Geology, 35*, 1123–1126.

Davidson, C., Rosenberg, C., & Schmid, S. M. (1996). Synmagmatic folding of the base of the Bergell pluton, Central Alps. *Tectonophysics, 265*, 213–238.

Davies, J. H., & von Blanckenburg, F. (1995). Slab breakoff: a model of lithosphere detachment and its test in the magmatism and deformation of collisional orogens. *Earth and Planetary Science Letters, 129*, 85–102.

Del Moro, A., Pardini, G. C., Quercioli, C., Villa, I., & Callegari, E. (1983). Rb/Sr and K/Ar chronology of Adamello granitoids, Southern Alps. *Memorie della Società Geologica Italiana, 26*, 285–299.

Diethelm, K. (1989). Petrographische und geochemische Untersuchungen an basischen Gesteinen der Bergeller Intrusion (Graubünden, Schweiz/Provinz Sondrio, Norditalien). Unpubl. Ph.D. Thesis, ETH Zurich, p. 183

Diethelm, K. (1990). Synintrusive basische Gänge und „endogene" Xenolithe: magma-mingling in der Bergeller Intrusion. *Schweizerische Mineralogische und Petrographische Mitteilungen, 70*, 247–264.

Fox, M., Reverman, R., Herman, F., Fellin, M. G., Sternai, P., & Willett, S. D. (2014). Rock uplift and erosion rate history of the Bergell Intrusion from the inversion of low temperature thermochronometric data. *Geochemistry, Geophysics, Geosystems, 15*, 1235–1257.

Galli, A., Le Bayon, B., Schmidt, M. W., Burg, J. P., Caddick, M. J., & Reusser, E. (2011). Granulites and charnockites of the Gruf Complex: evidence for Permian ultra-high temperature metamorphism in the Central Alps. *Lithos, 124*, 17–45.

Galli, A., Le Bayon, B., Schmidt, M. W., Burg, J. P., & Reusser, E. (2013). Tectonometamorphic history of the Gruf complex (Central Alps): exhumation of a granulite–migmatite complex with the Bergell pluton. *Swiss Journal of Geosciences, 106*, 33–62.

Galli, A., Le Bayon, B., Schmidt, M. W., Burg, J. P., Reusser, E., Sergeev, S. A., & Larionov, A. (2012). U–Pb zircon dating of the Gruf complex: disclosing the late Variscan granulitic lower crust of Europe stranded in the Central Alps. *Contributions to Mineralogy and Petrology, 163*, 353–378.

Geisler, T., Schaltegger, U., & Tomaschek, F. (2007). Re-equilibration of zircon in aqueous fluids and melts. *Elements, 3*, 43–50.

Giger, M., & Hurford, A. J. (1989). Tertiary intrusives of the Central Alps: their Tertiary uplift, erosion, redesposition and burial in the South-alpine foreland. *Eclogae Geologicae Helvetiae, 82*, 857–866.

Gregory, C. J., McFarlane, C. R. M., Hermann, J., & Rubatto, D. (2009). Tracing the evolution of calc-alkaline magmas: in-situ Sm–Nd isotope studies of accessory minerals in the Bergell Igneous Complex, Italy. *Chemical Geology, 260*, 73–86.

Gulson, B. L., & Krogh, T. E. (1973). Old lead components in the young Bergell massif, South-East Swiss Alps. *Contributions to Mineralogy and Petrology, 40*, 239–252.

Günther, D., von Quadt, A., Wirz, R., Cousin, H., & Dietrich, V. J. (2001). Elemental analyses using laser ablation-inductively coupled plasma-mass spectrometry (LA-ICP-MS) of geological samples fused with $Li_2B_4O_7$ and calibrated without matrix-matched standards. *Mikrochimica Acta, 136*, 101–107.

Hafner, M. (1993). Strukturgeologische und Geochemische Untersuchungen von Leukokraten Granit-Gängen und Migmatiten der Südlichen Adula am Monte Peschiera (Italia). Unpubl. Diploma Thesis, University of Basel, Basel.

Halliday, A. N., Stephens, W. E., & Harmon, R. S. (1980). Rb–Sr and O isotopic relationships in 3 zoned Caledonian granitic plutons, Southern Uplands, Scotland: evidence for varied sources and hybridization of magmas. *Journal of the Geological Society, 137*, 329–348.

Hammarstrom, J. M., & Zen, E. A. (1986). Aluminium in hornblende: an empirical igneous geobarometer. *American Mineralogist, 71*, 1297–1313.

Hanchar, J. M., & van Westrenen, W. (2007). Rare earth element behavior in zircon-melt systems. *Elements, 3*, 37–42.

Hinton, R. W., & Upton, B. G. J. (1991). The chemistry of zircon: variations within and between large crystals from syenite and alkali basalt xenoliths. *Geochimica et Cosmochimica Acta, 55*, 3287–3302.

Hoskin, P. W. O., & Schaltegger, U. (2003). The composition of zircon and igneous and metamorphic petrogenesis. In J. M. Hanchar & P. W. O. Hoskin (Eds.), *Zircon: reviews in mineralogy and geochemistry* (pp. 27–62). Washington: Mineralogical Society of America.

Irvine, T. N., & Baragar, W. R. A. (1971). A guide to the chemical classification of the common volcanics rocks. *Canadian Journal of Earth Sciences, 8*, 523–548.

Jaffey, A. H., Flynn, K. F., Glendenin, L. E., Bentley, W. C., & Essling, A. M. (1971). Precision measurement of half-lives and specific activities of ^{235}U and ^{238}U. *Physical Review C, 4*, 1889–1906.

Jäger, E., & Hantke, R. (1984). Evidenzen für die Vergletscherung eines alpinen Bergeller Hochgebirges an der Grenze Oligozän/Miozän. *Geologische Rundschau, 73*, 567–575.

Lee, C. T. A., Morton, D. M., Kistler, R. W., & Baird, A. K. (2007). Petrology and tectonics of Phanerozoic continent formation: from island arcs to accretion and continental arc magmatism. *Earth and Planetary Science Letters, 263*, 370–387.

Liati, A., Gebauer, D., & Fanning, M. (2000). U–Pb SHRIMP dating of zircon from the Novate granite (Bergell, Central Alps): evidence for Oligocene–Miocene magmatism, Jurassic/Cretaceous continental rifting and opening of the Valais trough. *Schweizerische Mineralogische und Petrographische Mitteilungen, 80*, 305–316.

Ludwig, K. R. (2000). *Isoplot/Ex. A geochronological toolkit for Microsoft Excel, version 2.2* (p. 56). Berkeley: Berkeley Geochronology Center Special Publication No. 1a.

Malusà, M. G., Villa, I. M., Vezzoli, G., & Garzanti, E. (2011). Detrital geochronology of unroofing magmatic complexes and the slow erosion of Oligocene volcanoes in the Alps. *Earth and Planetary Science Letters, 301*, 324–336.

Mattinson, J. M. (2005). Zircon U-Pb chemical abrasion (CA-TIMS) method: combined annealing and multi-step partial dissolution analysis for improved precision and accuracy of zircon ages. *Chemical Geology, 220*, 47–66.

McDonough, W. F., & Sun, S. S. (1995). The composition of the Earth. *Chemical Geology, 120*, 223–253.

Montrasio, A., & Trommsdorff, V. (1983). Guida all'escursione del massiccio di Val Masino-Bregaglia, Val Malenco occidentale, Sondrio. *Memorie della Società Geologica Italiana, 26*, 421–434.

Morand, P.C. (1981). Geologisch-petrographische Untersuchungen im südlichen Bergell: 1.Val Porcellizzo, Provincia di Sondrio, N-Italien. Unpubl. Diploma Thesis, ETH Zurich, p. 91.

Moticska, P. (1970). Petrographie und Strukturanalyse des westlichen Bergeller Massivs und seines Rahmens. *Schweizerische Mineralogische und Petrographische Mitteilungen, 50*, 355–446.

Mottana, A., Morten, L., & Brunfelt, A. O. (1978). Distribuzione delle terre rare nel massiccio Val Masino-Val Bregaglia (Alpi Centrali). *Rendiconti della Società Italiana di Mineralogia e Petrologia, 34*, 485–497.

Nandedkar, R. H., Ulmer, P., & Müntener, O. (2014). Fractional crystallization of primitive, hydrous arc magmas: an experimental study at 0.7 GPa. *Contributions to Mineralogy and Petrology, 167*(1015), 1–27.

O'Connor, J. T. (1965). A classification for quartz-rich igneous rock based on feldspar ratios. *U.S Geological Survey Professional Paper, 525B*, B79–B84.

Oberli, F., Meier, M., Berger, A., Rosenberg, C. L., & Gieré, R. (2004). U–Th–Pb and ^{230}Th/^{238}U disequilibrium isotope systematics: precise accessory mineral chronology and melt evolution tracing in the Alpine Bergell intrusion. *Geochimica et Cosmochimica Acta, 68*, 2543–2560.

Oschidari, H., & Ziegler, U. R. F. (1992). Vergleichende Sm-Nd- und Rb-Sr-Untersuchungen an Bergeller Geröllen aus der Gonfolite Lombarda („Südalpine Molasse") und an Bergeller und Novate Granitoiden des Ursprungsgebietes. *Eclogae Geologicae Helvetiae, 85*, 375–384.

Passerini, P., Sguazzoni, G., & Marcucci, M. (1991). Mesoscopic faults in the Bregaglia (Bergell) massif, Central Alps. *Tectonophysics, 198*, 53–72.

Reusser, C.E. (1980). Radiometrische Untersuchungen am Bergeller Granodiorit. Unpubl. Diploma Thesis, ETH Zurich, p. 101.

Reusser, C.E. (1987). Phasenbeziehung im Tonalit der Bergeller Intrusion (Graubünden, Schweiz/Provinz Sondrio, Italien). Unpubl. PhD. Thesis, ETH Zurich, p. 220.

Rosenberg, C. L. (2004). Shear zones and magma ascent: a model based on a review of the Tertiary magmatism in the Alps. *Tectonics, 23*, TC3002.

Rubatto, D., Hermann, J., Berger, A., & Engi, M. (2009). Protracted fluid-induced melting during Barrovian metamorphism in the Central Alps. *Contributions to Mineralogy and Petrology, 158*, 703–722.

Schmid, S. M., Berger, A., Davidson, C., Gieré, R., Hermann, J., Nievergelt, P., et al. (1996). The Bergell pluton (Southern Switzerland, Northern Italy): overview accompanying a geological-tectonic map of the intrusion and surrounding country rocks. *Schweizerische Mineralogische und Petrographische Mitteilungen, 76*, 329–355.

Schmidt, M. W. (1992). Amphibole composition in tonalite as a function of pressure: an experimental calibration of the Al-in-hornblende barometer. *Contributions to Mineralogy and Petrology, 110*, 304–310.

Schmitz, M. D., & Schoene, B. (2007). Derivation of isotope ratios, errors, and error correlations for U–Pb geochronology using ^{205}Pb–^{235}U–(^{233}U)-spiked isotope dilution thermal ionization mass spectrometric data. *Geochemistry, Geophysics, Geosystems, 8*, 1–20. doi:10.1029/2006GC001492).

Stacey, J. S., & Kramers, J. D. (1975). Approximation of terrestrial lead isotope evolution by a two-stage model. *Earth and Planetary Science Letters, 26*, 207–221.

Steiger, R. H., & Jäger, E. (1977). Subcommission on geochronology: convention on the use of decay constants in geo- and cosmochronology. *Earth and Planetary Science Letters, 36*, 359–362.

Stucki, A. (2001). High grade Mesozoic ophiolites of the Southern Steep Belt, Central Alps. Unpubl. PhD. Thesis, ETH Zurich, p. 167.

Sun, S. S., & McDonough, W. F. (1989). Chemical and isotopic systematics of oceanic basalts: implications for mantle composition and processes. In A. D. Saunders & M. J. Norry (Eds.), *Magmatism in the ocean basins* (pp. 313–345). London: Geological Society London.

Thomas, J. B., Bodnar, R. J., Shimizu, N., & Sinha, A. K. (2002). Determination of zircon/melt trace element partition coefficients from SIMS analysis of melt inclusions in zircon. *Geochimica et Cosmochimica Acta, 66*, 2887–2901.

Trommsdorff, V., & Connolly, J. A. D. (1996). The ultramafic contact aureole about the Bregaglia (Bergell) tonalite: isograds and a thermal model. *Schweizerische Mineralogische und Petrographische Mitteilungen, 76*, 537–547.

Trommsdorff, V., & Evans, B. W. (1972). Progressive metamorphism of antigorite schist in the Bergell tonalite aureole (Italy). *American Journal of Science, 272*, 423–437.

Trommsdorff, V., & Evans, B. W. (1977). Antigorite-ophicarbonates: contact metamorphism in Val Malenco, Italy. *Contributions to Mineralogy and Petrology, 62*, 301–312.

Trommsdorff, V., & Nievergelt, P. (1983). The Bregaglia (Bergell) Iorio intrusive and its field relations. *Memorie della Società Geologica Italiana, 26*, 55–68.

Vance, D., & O'Nions, R. K. (1992). Prograde and retrograde thermal histories from the central Swiss Alps. *Earth and Planetary Science Letters, 114*, 113–129.

Villa, I. M., & von Blanckenburg, F. (1991). A hornblende ^{39}Ar–^{40}Ar age traverse of the Bregaglia tonalite (South-East Central Alps). *Schweizerische Mineralogische und Petrographische Mitteilungen, 71*, 73–87.

Vogel, M. (2010). Petrography and geochemistry of lenses in upper Valle dei Ratti (Prov. Sondrio, Southern Alps, Italy). Petrographical and geochemical analyses of ultramafic, mafic and

calc-silicate lenses at the contact between the Bergeller tonalite and the Bellinzona-Dascio Zone in upper Valle dei Ratti. Unpubl. Master Thesis, ETH Zurich, p. 82.

Von Blanckenburg, F. (1989). Isotope geochemical and geochronological case studies of Alpine magmatism and metamorphism: the Bergell intrusion and Tauern Window. Unpubl. PhD. Thesis, ETH Zurich, p. 186.

Von Blanckenburg, F. (1992). Combined high-precision chronometry and geochemical tracing using accessory minerals: applied to the Central-Alpine Bergell intrusion (Central Europe). *Chemical Geology, 100*, 19–40.

Von Blanckenburg, F., & Davies, J. H. (1995). Slab breakoff: a model for syncollisional magmatism and tectonics in the Alps. *Tectonics, 14*, 120–131.

Von Blanckenburg, F., Früh-Green, G., Diethelm, K., & Stille, P. (1992). Nd-, Sr-, O-isotopic and chemical evidence for a two-stage contamination history of mantle magma in the Central-Alpine Bergell intrusion. *Contributions to Mineralogy and Petrology, 110*, 33–45.

von Quadt, A., Erni, M., Martinek, K., Moll, M., Peytcheva, I., & Heinrich, C. A. (2011). Zircon crystallization and the lifetimes of ore-forming magmatic-hydrothermal systems. *Geology, 39*, 731–734.

Wagner, G. A., Miller, D. S., & Jäger, E. (1979). Fission track ages on apatite of Bergell rocks from Central Alps and Bergell boulders in Oligocene sediments. *Earth and Planetary Science Letters, 45*, 355–360.

Wagner, G. A., Reimer, G. M., & Jäger, E. (1977). *Cooling ages derived by apatite fission-track, mica Rb–Sr and K–Ar dating: the uplift and cooling history of the Central Alps* (p. 28). Padova: Memorie degli Istituti di geologia e mineralogia dell'Università di Padova.

Weibel, M. (1960). Chemismus und Mineralzusammensetzung von Gesteinen des nördlichen Bergeller Massivs. *Schweizerische Mineralogische und Petrographische Mitteilungen, 40*, 69–93.

Wenk, H. R. (1973). The structure of the Bergell Alps. *Eclogae Geologicae Helvetiae, 66*, 255–291.

Wenk, H. R., Hsiao, J., & Flowers, G. (1977). A geochemical survey of granitic rocks in the Bergell Alps. *Schweizerische Mineralogische und Petrographische Mitteilungen, 57*, 233–265.

Zorpi, M. J., Coulon, C., Orsini, J. B., & Cocirta, C. (1989). Magma mingling, zoning and emplacement in calc-alkaline granitoid plutons. *Tectonophysics, 157*, 315–329.